King Saud University

Arabian Journal of Chemistry

www.ksu.edu.sa
www.sciencedirect.com

ORIGINAL ARTICLE

Synthesis and application of treated activated carbon for cationic dye removal from modelled aqueous solution

Rumi Goswami, Amit Kumar Dey *

Department of Civil Engineering, Central Institute of Technology Kokrajhar, Assam 783370, India

Abstract Use of activated carbon (AC) prepared from rice husk and treated with anionic surfactant is investigated to eliminate cationic dye crystal violet (CV) using modelled dye solution. AC modified with anionic surfactant sodium lauryl sulfate (ACSLS) and other two surfactant namely sodium dodecyl sulfonate and hexadecyl trimethyl ammonium bromide were used for the analysis. Optimum ACSLS was analyzed and characterized using BET, XRD, SEM accompanied with XEDS, FTIR, HR-TEM and zeta potential, which confirms the sorption of CV onto ACSLS. Influence of pH, dose of adsorbent, concentration of initial dye, contact time, additive salts as well as actual water samples were investigated. Presence of NH^{4+}, Ca^{2+}, Mg^{2+}, Na^{2+}, Ca^{2+} and K^+ cations in dye solution were having negligible (less than 4 %) influence on dye removal capacity. Study of mass transfer parameters revealed intra particle diffusion and film diffusion both played their part, whereas other kinetic studies has shown that experimental data fitted best with Pseudo 2nd order rate. Isotherm studies accompanied with error analysis revealed that Langmuir isotherm controls the adsorption equilibrium with highest capacity of CV adsorption with optimum operating conditions as pH = 6, temperature = 318 K, adsorbent dose = 100 mg/L and dye concentration = 30–60 mg/L. Study of thermodynamics and temperature analysis have shown that the sorption reaction was favourable and spontaneous with rise in temperature and endothermic in nature. Column studies are reported for varying rate of flow, depth of bed and dye concentrations along with analysis of column experimental data with various models like Yoon-Nelson, Thomas, Bohart-Adam and Clark model. Reusability (no. of cycles) of used adsorbent was studied using regeneration experiments. Analysis inferred that AC modified using surfactants can be a useful technique for enhanced adsorption capacity of dyes from aqueous solution and not much work has been

* Corresponding author.
  E-mail addresses: rumi.goswami12@gmail.com (R. Goswami), ak.dey@cit.ac.in (A. Kumar Dey).
Peer review under responsibility of King Saud University.

Production and hosting by Elsevier

reported on use of anionic surfactant modified AC for dye removal process.

1. Introduction

One of the biggest environmental problems is the increasing presence of dyes in aquatic bodies. The dyes do not naturally degrade; therefore, their persistence prevents light from penetrating water and harms the ecology (Alhogbi et al., 2021; Wong et al., 2004). The effluents from the textile, paint, medicinal, and biotechnology industries as well as other industries contribute to the introduction of cationic crystal violet (CV) dye into aquatic systems. It is well known that CV is mutagenic, teratogenic, and mitotically poisonous. The use of bio sorbent to absorb the dye from waste water was shown to be the most practical strategy among the various dye removal methods (Tan et al., 2008). Industrial pollutants affect both groundwater and surface water, as well as human health, making them one of the major environmental challenges (Foroutan et al., 2021; Verma et al., 2012; Peighambardoust et al., 2021). For the treatment of wastewater from the dye industry, a number of technologies have been documented, including enhanced oxidation, membrane filtering, microbial technologies, bio-electrochemical degradation, and photocatalytic degradation (Yu et al., 2010; Alventosa-deLara et al., 2012; Yagub et al., 2014; Sun et al., 2010). Because of its effectiveness, affordability, capacity to separate a variety of chemical compounds, and ease of use, adsorption employing various adsorbents is preferable to other separation procedures. Due to its low cost, environmental friendliness, and renewable nature, agricultural waste has been the subject of a lot of research in recent years (Karaca et al., 2008). Activated carbon (AC), the most widely used adsorbent, is primarily used to remove both organic and inorganic pollutants from water. A key parameter for determining the adsorption impact of an adsorbent is its capacity for adsorption. For the elimination of CV dye, a number of low-cost adsorbents, such as grapefruit peel (Wang et al., 2018), rice husk (Abdel-Fattah et al., 2015; Dey and Kumar, 2017), jackfruit leaf powder (Hailu et al., 2017), ginger waste (Jiménez-Castañeda and Medina, 2017), etc., have been utilised. Activated carbon (AC) was utilised as wood charcoal for a very long time. The medical industry uses activated carbon for a variety of purposes, including as a purifying agent. In the past, charcoal was employed as a filter medium in India to purify water. In 1900, activated carbon was used for the first time in the sugar refining industry. Due to its substantial surface area, high porosity, and enhanced surface response, activated carbon is employed for adsorption. The effectiveness of activated carbon has been demonstrated in the treatment of leachate, the removal of heavy metals from aqueous solutions, including cadmium (II), lead, and chromium (Behrouz et al., 2018).

To modify AC, several physical, chemical, and biological methods are used. The alteration of surfactants is a crucial AC chemical modification technique. The method of modification by surfactant for activated carbon can increase the dispersion and hydrophobicity of AC in water due to a strong interaction between water and activated carbon and a decrease in the binding energy between particles. Surfactant has the advantages of being affordable and it is less harmful to AC structure. Surfactant can also change the surface charge characteristics of AC and produce more ionic adsorption sites for pollutants, which increases the capacity of ionic pollutants to bind to AC (Reis et al., 2021) and encourages selective adsorption. In wastewater treatment, AC modified with a surfactant as an adsorbent is used to remove impurities such as heavy metals (Dey et al., 2018; Lin et al., 2013), pollutants (organic) (Choi et al., 2008; Namasivayam and Suresh Kumar, 2008), and reactive dyes (Zhou et al., 2018; Dey and Dey, 2021; Fu et al., 2015; Wu and Pendleton, 2001). One such safe anionic surfactant is sodium lauryl sulphate.

When we talk of novelty of the present study reported with this work, we would like to highlight that the effect of AC modified by surfactant on inorganic metal ions has been the subject of numerous investigations, however the study on adsorptive removal of organic cationic dye using anionic surfactant modified AC has been relatively understudied. Previous research has shown that different surfactants added to AC have different impacts on dye wastewater with different water qualities. It is crucial to understand how the presence of other ions influences adsorption as a result. Further information is required to completely understand the adsorption behaviour of CV dye on modified AC in the interim. In the current work, the potential for employing anionic surfactant-modified AC to extract cationic dye CV from aqueous solution was investigated. AC modified with anionic surfactants such as sodium dodecyl sulfonate (ACSDS), sodium lauryl sulfate (ACSLS) and hexadecyl trimethyl ammonium bromide (ACHTAB) were used as adsorbents for potential removal of CV dye. Also, as the main motive of the present work is to remove cationic dye from aqueous solution, hence an anion influenced adsorbent was adopted for the adsorption process.

2. Materials and methods

2.1. Materials

Hexamethyl paraaminobenzoyl chloride, popularly known as crystal violet or gentian violet, is a triarylmethane dye used for Gram bacterial categorization and histology staining. It was once crucial as a topical preservative and possesses antibacterial, antifungal, and insect repellent qualities. The World Health Organization still lists the dye, but more recent medications now predominate in its medicinal use. Although it is now frequently used as a synonym for crystal violet, gentian violet was initially called for a mixture of methyl-p-nitroaniline dye (methyl violet). Similar to some gentian flower petals, the term alludes to the colour. Crystal violet ($C_{25}N_3H_{30}Cl$), which has a molar mass of 407.99 g/mol, was utilized as an adsorbent instead of gentian or violet. SLS ($C_{12}H_{25}SO_4Na$), SDS ($C_{12}H_{25}SO_3Na$), and hexadecyl trimethyl ammonium bromide (HTAB) were the surfactants used in this experiment. Calcium chloride, sodium chloride, hydrochloric acid, magnesium sulphate heptahydrate, sodium hydroxide, sodium nitrite, potassium chloride, potassium hydroxide, potassium chloride, and ferrous sulphate were among the additional compounds used. The chemicals are all bought from Himedia, India. The process of chemical activation was utilized to create AC from rice husk (RH). From Himedia, analar grade CV dye was also purchased. The molecular makeup of CV dye is displayed in figure S1.

2.2. Activated carbon preparation

Activated carbons (ACs) were prepared from rice husk as following procedures: firstly, the rice husks were washed with water to remove dirt and other contaminants, oven-dried at 110 °C for 12 h then grounded and sieved to fractions with average particle size of 1.0 mm. Secondly, the prepared husks were carbonized at 400 °C under nitrogen flow (300 mL min^{-1})

for 90 min. The resulting samples were impregnated with NaOH and water with a weight ratio of 1/3 and dried at 120 °C for 12 h. Then, the preparative process was followed by heating at 400 °C for 20 min under nitrogen atmosphere at a flow rate of 300 mL min^{-1}; thereafter the temperature was raised to the predetermined temperature of 800 °C at a heating rate of 10 °C and maintained at the final temperature for 60 min to activate the obtained material. Finally, the activated product was grounded, neutralized by 0.1 M HCl solution and washed several times with hot distilled water to a constant pH (6.6–7.0). The washed activated carbon samples were dried under vacuum at 120 °C for 24 h and stored in a desiccator. The final sample obtained is the activated carbon prepared at 800 °C (Dey and Kumar, 2017; Yagub et al., 2012; Kannan and Sundaram, 2001).

2.3. Modified activated carbon

5 g of activated carbon and 8.60 mM anionic surfactant SLS were added to 100 mL of aqueous solution. The AC was shaken at 308 K for 6 h before being filtered and rinsed with deionized water. The filtered AC was then held in a sealed and dry environment after drying for 24 h at 318 K in an air-dry oven. Adsorption has been shown to be most effective at the surfactant concentration that corresponds to the critical micelle concentration (CMC) (Dey and Dey, 2021). According to published data, SLS has a CMC of 8.60 mM at a temperature of 28 °C. The labels ACR and ACSLS, respectively, were assigned to the untreated AC and the AC modified with anionic surfactant SLS. The SDS and HTAB, which were used to modify AC in a similar manner at a concentration of 1 CMC, were given the names ACSDS and ACHTAB, respectively.

2.4. Characterization studies

Brunauer-Emmett-Teller (BET) analysis is used to determine the surface area, pore volume and pore size distribution of an ACSLS with an automatic adsorption–desorption system (BELSORP-mini II, BEL Japan Inc.), based on N$_2$ adsorption data at −196 °C. In order to understand the nature of X-ray diffraction (XRD) and determine the structure of the underlying crystal of the adsorbent, an X-ray diffractometer instrument (X-ray 6100 Shimadzu-Japan) was utilised. The Bragg angle (θ) was measured across a range of 5° to 90° and at a rate of 5° per minute. Environmental scanning electron microscopy (SEM) was used to examine the surface morphology of the adsorbent (Make: FEI, Model: Quanta 200, with 3 nm resolution at 30 kV, ESEM mode), along with energy dispersive X-ray spectroscopy for elemental analysis (XEDS). The samples were coated with gold using a sputtering coater (model: S150B, Edwards High Vacuum ltd., England) for XEDS analysis in order to prevent the creation of local electrical charges. Fourier transform infrared spectroscopy (FTIR) was carried out using a device made by Bruker, Germany, model 3000 hyperion microscope with vertex 80 FTIR system and array for focal plane 128 × 128, range 900–4000 cm^{-1}, to identify the functional groups in charge of sorption. High resolution transmission electron microscopy (HR-TEM 200 kV, make: JEOL, model: JEM 2100F at 200 kV) was used to investigate pore size and the development of adsorption layers. Zeta potential and

zero point of charge (pH$_{PZC}$) analysis procedure is discussed using supplementary discussion section S1in the supplementary materials and is used to find the stable pH value for the sorption process and net surface charge of the adsorbent (ACSLS).

2.5. Mass balance method for batch analysis

At the maximal absorbance peak for CV, a UV/visible spectrophotometer (PerkinElmer Lambda 45) was utilised to examine the removal of CV using surfactant-modified activated carbon (590 nm). The rate of adsorbate removal (adsorption capacity) was calculated using the mass balance on dye concentration (Eq. (1)):

$$Q_e = \frac{C_0 - C_e}{m} V \tag{1}$$

Q$_e$ is adsorption capacity at equilibrium (mg/g), C$_0$ and C$_e$ are the corresponding concentrations of dye at the initial and equilibrium stage, volume of CV dye solution is presented as V in litre and m is the mass of ACSLS ingrams.

Dye (CV) removal % was found out using Eq. (2) (Dey et al., 2022):

$$\text{Percent Removal of CV dye} = \frac{C_0 - C_e}{C_0} \times 100 \tag{2}$$

Using laboratory studies, it was discovered how several experimental variables such as pH (2–9), initial CV concentration (30, 60, 90 mg/L), contact time (0–180 min), adsorbent dosage (5–100 mg), temperature (298, 308, 318 K), and ionic salts influenced CV adsorption onto modified AC. The initial pH of the solution was determined using a pH metre along with a 0.1 M solution of sodium hydroxide (NaOH) and hydrochloric acid (HCl). A specific quantity of treated AC was added to a conical flask with a capacity of 250 mL, along with 100 mL of solution containing various concentrations of CV. At the proper intervals, each combination was rotated at a speed of 125 RPM and a temperature of 25 °C. The materials were then filtered and evaluated after adsorption. The right quantity of CV was dissolved in distilled water to create the CV(1 g/L) stock solution. CV concentrations were determined using UV–Visible spectrophotometer (PerkinElmer lambda 45) at λ^{max} = 590 nm. Average value of three-time experimental data was adopted for the analysis and interpretation.
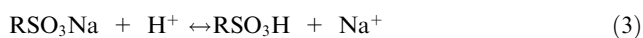
3. Results and discussion

3.1. Surfactants effect and adsorption mechanism

Figure S2 shows the degree of CV adsorption onto AC modified with different surfactants in aqueous solution at a concentration of CV of 100 mg/L. ACSLS showed the highest adsorption capacity and soonest, followed by ACR, ACSDS, and ACHTAB in the observation of the favorability of dye adsorption capacity by different surfactants. Figure S2 demonstrates that ACHTAB had the least amount of CV dye adsorption when compared to ACSLS and ACSDS. Because HTAB is a cationic surfactant, it had an antagonistic attraction to the cations of dye and the adsorption sites that were already occupied on AC, which reduced the ability of cationic CV dye adsorption. When compared to untreated carbon, surfac-

tants on AC may narrow the pores of the carbon, reducing its ability to absorb CV. Compared to untreated AC surfaces, surfactant-loaded AC has a larger manufacturing capacity of ion exchange sites and a stronger attraction for CV. More CV adsorption on ACSLS compared to ACR has demonstrated that the positive influence of the ACSLS functional group counter outweighed the negative impact of pore blockage, while less CV removal by ACSDS compared to ACR has demonstrated that the negative impact of pore blockage counter outweighed the positive influence of the ACSDS functional group.

The high CV dye adsorption capacity of AC treated with anionic surfactants is a result of the strong bonding between the cationic CV dye and anionic surfactant. The chemical properties of the functional groups in the surfactant have an impact on adsorption. In a solution containing the dye ion, the sodium ions (e.g., $R-SO_3^-$ H^+) and protons (e.g., $R-SO_3^-$ H^+) bound to the strong acid conjugate base of SLS can be easily diluted and replaced (Eren and Acar, 2006). The ACSLS exhibited a strong CV elimination impact as a result. Because there was less of a connection between the SDS functional group and the CV dye than there was with the SLS functional group, ACSDS had a lesser adsorption impact on CV than ACSLS. The possible sorption pathway for the chemical adsorption of CV onto ACSLS is shown in Figure S3. According to equations (3) and (5), reactions between the CV dye cation (M^+) and RSO_3Na may have occurred on ACSLS. The carboxyl, phenolic hydroxyl on AC is represented by ROH, whereas the active group of SLS that tends to dissolve in water is RSO_3Na.

$$RSO_3Na \ + \ H^+ \leftrightarrow RSO_3H \ + \ Na^+ \tag{3}$$

$$RSO_3Na \ + \ M^+ \leftrightarrow RSO_3M \ + \ Na^+ \tag{4}$$

$$ROH \ + \ M^+ \leftrightarrow ROM \ + \ H^+ \tag{5}$$

3.2. Characterization studies

Scanning electron microscopy (SEM) was used to examine the adsorbent surface structure. The surface morphology and elemental characteristics of the adsorbent are shown in detail in Fig. 1. Fig. 1a shows an ACR surface with micropores of varied widths and a moderate amount of carbon detritus. Fig. 1b shows the ACSLS surface for a significant number of undulations and a significant amount of trash component filling the pores in contrast to untreated AC. This resulted from the electrostatic interaction and adhesion of SLS molecules. The pores were heavily clogged with material debris, which may have reduced surface area but also provided ion exchange sites for adsorption. The SEM picture of ACSLS following CV dye adsorption is shown in Fig. 1c, and it can be seen that the CV dye particles adhered to the surface of the material. Fig. 1 (d-f) illustrates the elemental analysis of ACR, ACSLS and ACSLS following CV adsorption using XEDS analysis. Fig. 1d shows the elemental present in the untreated AC where C, O and Na elements can be observed. Following treatment with the anionic surfactant SLS, the presence of Cu components was also noted (Fig. 1e), which may be related to the surface modification of the raw activated carbon with surfactant. After dye adsorption, Fig. 1f demonstrates the substitution of

Na elements with Rb and Hg components, though in variable proportions, suggesting a change in the shape of the adsorbent surface following dye adsorption. According to the study, ACSLS-CV composites were created following CV sorption, which is proof that CV adsorption occurred. Fig. 1 illustrates the simultaneous presence of several components on the adsorbent surface at various stages (d, e, f). Similar sorption phenomena have been described in the past.

Figures S4a and S4b show the XRD patterns for ACSLS and CV loaded ACSLS. As many as 13 distinct and sharp peaks can be seen in the XRD pattern of ACSLS in S4a at various θ values (28.8°, 36.4°, 37°, 38.7°, 42.9°, 43.9°, 45.1°, 54.6°, 60.9°, 66.6°, 72.9°, 79.1° and 83.1°), which may be the result of the inclusion of higher ion exchange sites and Now that we have compared S4a and S4b, we can see a clear difference between ACSLS before and after dye adsorption in terms of peak shift, peak number, and peak intensity. The significant decrease, shift, and disappearance of peaks following dye adsorption (shown in figure S4b) supported CV adsorption. As opposed to 14 such crystalline peaks prior to adsorption, there were only 9 peaks remaining after adsorption at varied θ values (37°, 38.6°, 43.9°, 42.4°, 54.8°, 67.8°, 71.9°, 79° and 83.2°). While the peak's shifting after adsorption suggests that the unit cell is contracting as a result of the CV dye molecules occupying the sorbent structure, the disappearance and reduction in the intensity and number of peaks suggests that the adsorbent structure's crystallinity may be being lost as a result of dye adsorption.

FTIR research was carried out to identify the several functional groups in charge of the CV adsorption process. FTIR is a great tool for identifying and understanding functional groups. At the research facility SAIF Bombay in India, routine spectrum analysis was carried out. In Section 2.4 of this report, the features of the instrument are discussed. The FTIR spectra of ACSLS before and after CV adsorption are shown in Fig. 2a and 2b. Due to the connected hydroxyl or amine groups, the broad band and strong band for ACSLS were seen at 3433.57 cm^{-1}, as shown in Fig. 2a. The value obtained from the –CH asymmetric stretching was 2927.98 cm^{-1}. The peak value for the carboxyl group stretching vibration was 1711.41 cm^{-1}. The asymmetric and symmetric stretching vibrations of C=O groups were attributed to the bands at 1612.12 cm^{-1} and 1382.32 cm^{-1}. Alcohols and carboxylic acids can be stretched C—O along the band at 1100.12 cm^{-1}. The symmetrical stretching vibration bands of hydroxyl or amine groups were displaced from 3433.57 cm^{-1} to 3412.23 cm^{-1} after the adsorption, as shown in Fig. 2b. Carboxyl group stretching bands were moved from 1711.41 cm^{-1} to 1630.52 cm^{-1}, and stretching bands from 1612.12 cm^{-1} and 1382.32 cm^{-1} were moved to 1426.09 cm^{-1} and 1056.19 cm^{-1} respectively.

Similar changes were made to C—O peak, which moved from 1100.12 cm^{-1} to 1031.44 cm^{-1}, respectively. The analysis of FTIR spectra revealed that most significant bands decreased in size and shifted in intensity following dye adsorption (hydroxyl group decreased from 3433.57 cm^{-1} to 3412.23 cm^{-1} and carboxyl group increased from 1711.41 cm^{-1} to 1630.52 cm^{-1}) as a result of dye molecules filling ionized sites. Additionally, there was shifting and the appearance of several other peaks following adsorption, demonstrating the successful accumulation of CV dyes onto ACSLS surface.
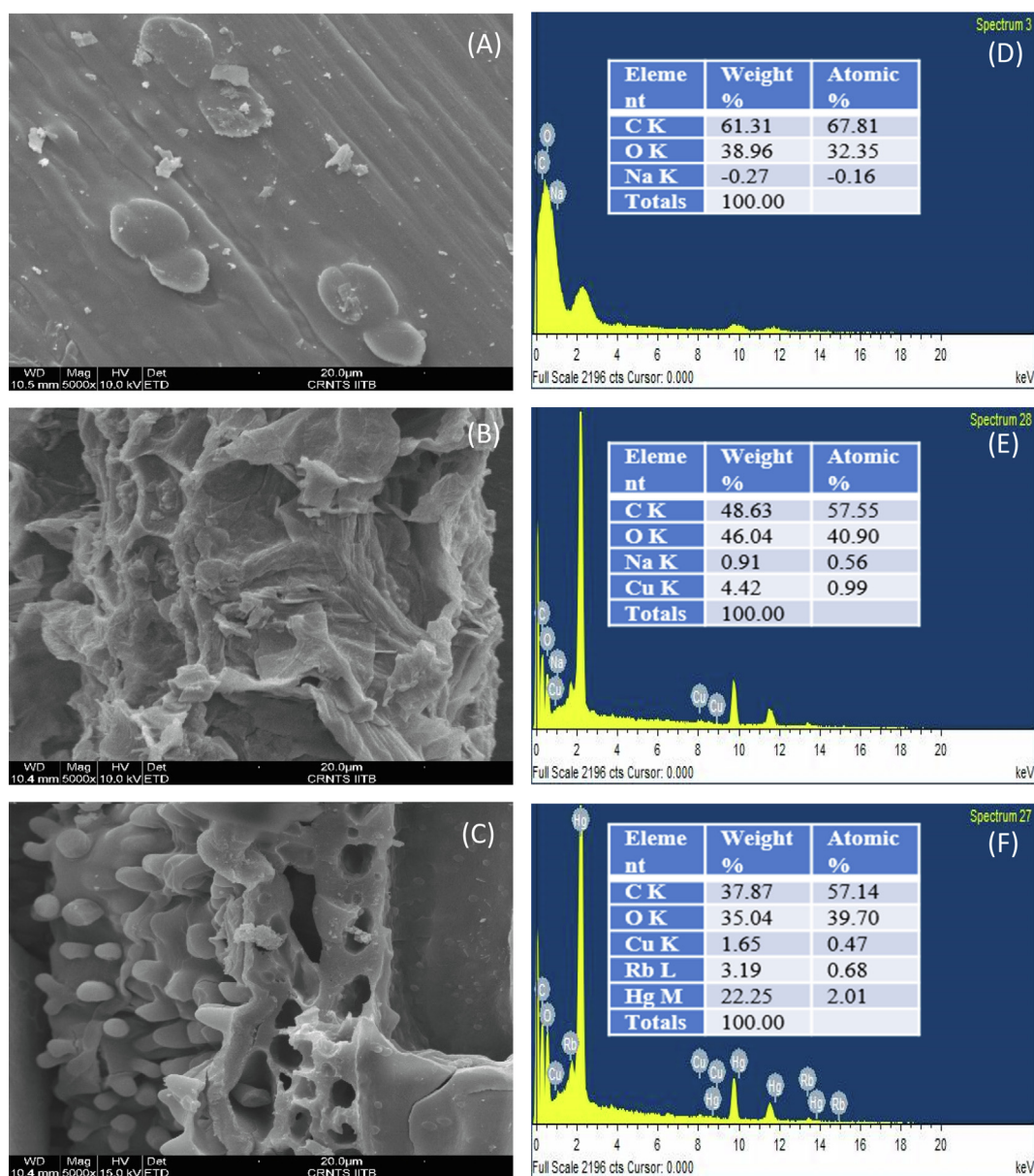
Fig. 1 SEM mages for **(a)** ACR **(b)** ACSLS. **(c)** ACSLS after dye adsorption and XEDS images for **(d)** ACR **(e)** ACSLS **(f)** ACSLS after dye adsorption.

The HR-TEM analysis was used to demonstrate the adsorption of CV molecules on the ACSLS surface by analyzing the ionization active sites/pores and their diameters, magnifying the adsorbent surface, and confirming the accumulation of adsorbate layer formation over the adsorbent. As seen in figure S5a, the pores on the AC surface may have been filled with ionized debris as a result of the SLS alteration, but the presence of the debris itself provided the ionization active sites necessary for effective dye adsorption. As shown in figure S5b, the dark spots are the result of CV dye molecules being deposited on the surface of the ACSLS. Therefore, the results of the HR-TEM investigation support those of the BET, XRD, FTIR, and SEM characterization studies. Figure S5b, which depicts a magnified sample adsorbed site, shows the average pore size following adsorption as 23.6 nm, which is consistent with the BET analysis.

BET analysis was carried out using a variety of models to determine the pore volume, average pore radius, and adsorbent surface area. To estimate surface area, 25 mg of adsorbent were degassed at 300 °C for 3 h. The process took about 24 h to complete. The principal pore size distribution of the adsorbent is shown in the distribution of pore size curve created (figure S6) using the Barrett-Joyner-Halenda (BJH) analysis, and the complete adsorption and desorption data are presented in Tables S1 and S2. A typical I-type isotherm was exposed via adsorption and desorption phenomena. Prior to adsorption, the adsorbent area of the surface was 195.42 m^2/g, and it was 206.34 m^2/g after adsorption. To obtain the surface area in the 0.05–0.95p/p$_0$ range, multipoint BET was utilized. It confirms that after CV dye adsorption, the adsorbent's surface area increases, showing a clear reduction in pore size brought on by the accumulation of CV dye in the adsorbent's pores
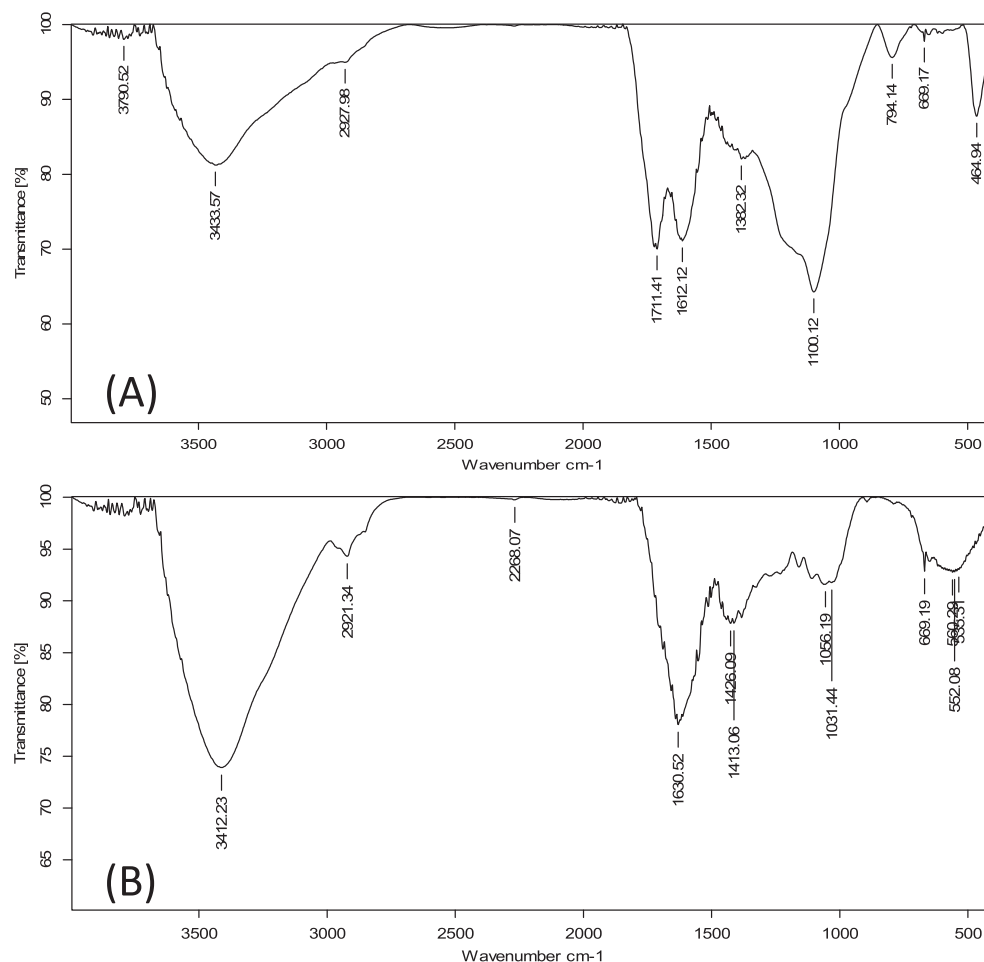
Fig. 2 FTIR routine spectrum for **(a)** ACSLS before adsorption **(b)** CV loaded ACSLS.

(Dey and Goswami, 2022). A specific alteration in the adsorbent's morphology brought about by dye adsorption increased surface area and decreased adsorbent pore size. Increased surface area favours the structural modification that takes place during the adsorption process (Dey and Goswami, 2022). The majority of the pores are focused in the region of less than 35 nm, which suggests that the ACSLS was behaving like nanoparticles with extremely small pore diameters and mesoporous materials with a large specific surface area.
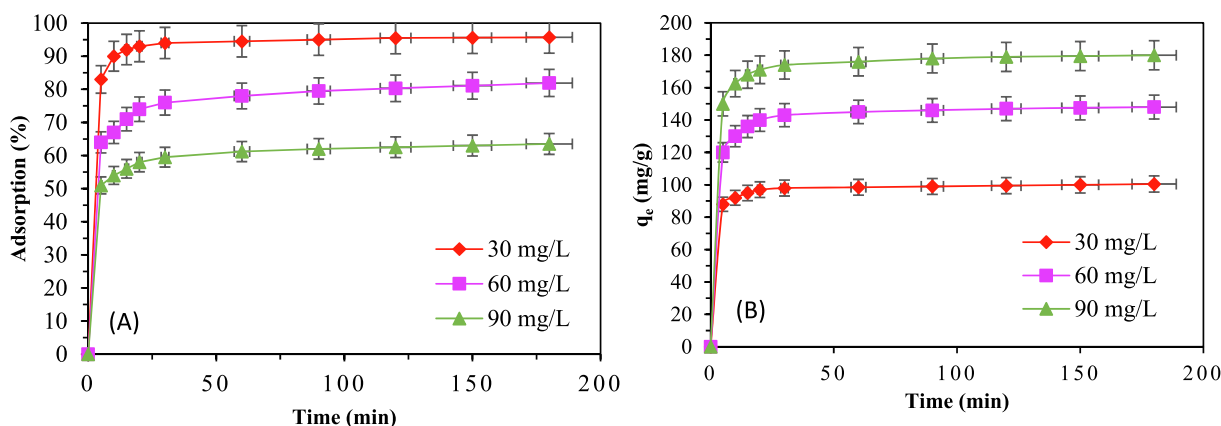
3.3. Effect of contact time

In the process of organic dye adsorption, contact time is crucial. Where the contact time can enhance the effectiveness of the treatment and show the most economical path. For three initial CV concentrations (30, 60 and 90 mg/L), the effect of contact time of organic dye adsorption on AC-ACSLS was therefore tested. Fig. 3 shows the relationship between the rate of adsorption and the capacity of CV on ACSLS and time. Fig. 3 demonstrates that as contact duration rose, elimination capacity and capacity of CV by ACSLS increased as well, eventually reaching a maximum value. The procedure was split into two halves. To attain the relative adsorption equilibrium condition known as rapid adsorption, the first stage required 5–30 min. The interactive process between CV dye and the active sites of adsorption was responsible for this performance,

and the ACSLS adsorbent functional groups were entirely and effectively completed. For the first halve, the pace at which the dye was adsorbed onto the sorbent surface regulated the absorption rate. The second phase was the slow adsorption process. After 30 min of contact time, the relative increase in CV removal extent was negligible, and as time went on, the adsorption rate decreased until it eventually stabilized. As sorbate molecules bound to sorbent surface ionization sites, the functional groups of the ACSLS adsorbent eventually became saturated. With accessible pores existing on the surface of the sorbent, dye transfer from the outer border to the inner site happened in the second half, which ultimately influenced the adsorption capacity and rate (Dey et al., 2022). Additionally, the time it took to reach adsorption equilibrium increased with the starting dye concentration. The results largely agreed with past studies on dye clearance rates (Dey and Dey, 2021). For the studies that followed, a contact time of 120 min was selected based on the link between contact length and CV removal.

3.4. pH effect on dye adsorption capacity

The pH factor is recognized as one of the most significant factors impacting the adsorption processes because of its effects on both the adsorbent surface charge and the adsorbate. Adsorption studies were conducted for dye concentration val-

Fig. 3 Influence of contact time for CV adsorption onto ACSLS (**a**) sorption percentage (**b**) sorption capacity, with ACSLS dose = 100 mg/L, T = 318 K and pH = 6.0.

ues of 30, 60 and 90 mg/L for a pH range of 2–9 in order to examine the impact of pH on CV adsorption on ACSLS. The capacity of CV to adsorb onto ACSLS and its removal percentage are both shown in Figure S7 as functions of pH. Figure S7a shows how the alkaline condition was beneficial for CV adsorption on ACSLS. Figure S7b shows the adsorption capacities of CV at various pH values. For dye concentration of 60 mg/L, adsorption capacities for the pH range of 2–9 are noted as 127.21, 132.92, 137, 143.12, 145.96, 152.76, 158.23, 160.1 and 162 mg/g respectively which signifies that raising the pH value improved both the adsorption removal and adsorption capacity of CV adsorption. The pH levels of the dye solution determine the degree of ionization of both acidic and basic substances as well as the charges present at the surface of ACSLS (Lagergren, 1898). At lower pH levels, functional groups with oxygen on ACSLS would not dissolve hydrogen ions (H^+) and SLS-electronegativity AC's and the electrostatic interaction between ACSLS and dye cation would not be as strong. Additionally, free hydrogen ions might have reduced the rate of CV elimination by competing with the dye cation for adsorption on the AC site, delaying dye cation adsorption. As the amount of hydroxide ions in the solution increased, the dissociation degree of CV reduced, and as a result, the rate of CV elimination increased as the pH value rose (Ho and McKay, 1999). Additionally, as pH increased, the functional groups with oxygen on the ACSLS surface enhanced the degree of H^+ dissociation, increasing ACSLS electronegativity and the force of the electrostatic interaction between ACSLS and the dye cation (Wu and Pendleton, 2001). In addition, when the pH is high, O—H groups and C=O groups on the surface of the adsorbent can seize cationic dye molecules (Ho et al., 2005).

The same has been supported by FTIR analysis (Fig. 2a and 2b), where the shifting and contracting of O—H and C=O groups upon adsorption make it clear. As a result, ACSLS has a high CV adsorption performance in an alkaline environment. The results are comparable to those previously reported (Karaca et al., 2008). Another investigation (Dey et al., 2022) indicated that the rate of cationic dye adsorption by leaves of raw pine charcoal was more effective at higher pH levels than it was at lower pH levels. Between pH 7 and 9, the rate of adsorption increased very little. It increased dramatically between pH 2 and 7.

In the supplemental discussion section S1, the zeta potential and method for determining the point of zero charge are covered. Figure S8a displays the variation in zeta potential values for ACR and ACSLS with regard to pH. The estimated values for ACSLS and ACR were 3.45 and 4.68, respectively. A study revealed that ACSLS had a higher surface electronegativity than ACR, which was explained by the hydrophobic alkyl end of the surfactant's vander Waals force connection to the surface of activated carbon (non-polar). SLS was applied to functional groups like phenolic-hydroxyl and carboxyl present on the surface of AC in order to reduce the amount of dissociated H^+. Compared to ACR, ACSLS has a stronger electrostatic affinity and adsorption capability toward CV because of its higher electronegativity. In this study, the pH ranged from 4 to 7, and the rate of CV adsorption on ACSLS was generally constant. The ACSLS complex's positive and negative pH (pH_f- pH_i) measurements were assessed and plotted in relation to the starting pH. (pH_i). Plot revealed that pH was zero at starting pH of 5.42 (i.e., pH_{PZC} = 5.42). (refer figure S8b). As a result, when the solution has a pH more than 5.42, as mentioned in section S1 of this report, the surface of the ACSLS complex will be negatively charged and capable of absorbing the cationic dye (Eren and Acar, 2006; Biswas et al., 2009). Based on the zeta potential and pH_{PZC} analyses, a pH of 6.0 was considered for different studies carried out for the present work.

3.5. Effect of adsorbent dose

Dose of adsorbent has a remarkable impact on the activity of adsorption. The impact of dose of adsorbent on adsorption of CV adsorption investigated to obtain the optimal quantity of adsorbent at different concentrations of CV (Dey et al., 2022). As illustrated in Fig. 4, 100 mL of CV solution having three variety of concentrations (30, 60 and 90 mg/L) were tested with different adsorbent dosages (5–100 mg). Under varied CV concentrations, a similar pattern in CV adsorption pattern on ACSLS was found. Because the number of adsorbent pores and adsorption sites grew due to increase in sorbent quantity, CV removal rate steadily enhanced.

The adsorption would tend toward equilibrium when the adsorbent mass reached a specific value. The CV removal rate
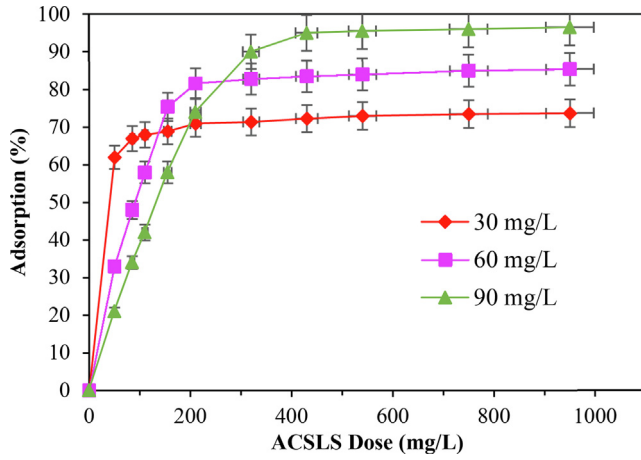
Fig. 4 Influence of ACSLS dose for CV sorption (time = 120 min, pH = 6.0, T = 318 K).

began to saturate at adsorbent masses of 40, 45, and 60 mg, which correspond to initial CV concentrations of 30, 60 and 90 mg/L, respectively. High adsorbent doses resulted in an equilibrium state of the surface and a decrease in the capacity of adsorption per unit adsorbent mass because the number of molecules of CV dye present in the aqueous mix was inadequate to fully mix with all influential sites of adsorption on the adsorbent.

3.6. Influence of dye concentration

To examine how the initial dye content impacts the adsorption capacity of ACSLS, four different initial concentrations of CV (30, 60, 90 and 120 mg/L) were used along with 5 to 100 mg of ACSLS. Adsorbent samples weighing 20 mg were added to a dye solution containing 100 mL, where they remained for 120 min at 318 K. The experimental results are shown in Table 1.

According to the results shown in Table 1, as the starting dye concentration was increased from 30 to 120 mg/L, the sorption rate (percent) of CV by 20 mg of ACSLS adsorbent decreased from 97.3 to 74.3 percent, but at the same time, the equilibrium capacity of adsorption (q_e) increased from 65.9 to 173.1 mg/g. Additionally, when the dye concentration was 90 mg/L, the maximum capacity of adsorption at equilibrium (q_e) was discovered to be up to 173.1 mg/g. The findings showed that the amount of adsorption of AC at 90 mg/L was equivalent to that at 120 mg/L because the sites of adsorption of the adsorbent became fully adsorbed when the concentration of CV climbed above 90 mg/L. Due to a lack of readily available high concentration CV active sites, dye removal

extent decreased as initial CV concentration increased (Onal, 2006), but ACSLS's ability for CV adsorption improved as initial CV concentration increased. SLS's sulphate functional group provided favourable ion exchange sites for CV ion adsorption. When compared to untreated AC, activated carbon augmented with an anionic surfactant displays more adsorption sites with positive charges and a robust adsorptive activity for removing cationic dye (Wang et al., 2018; Dey and Kumar, 2017).

3.7. Adsorption isotherm studies

The importance of the adsorption isotherm in explaining how the adsorbent will interact with the adsorbate and providing a sense of adsorption capacity cannot be overstated. They are crucial to comprehending the adsorption mechanism. It can be assumed of the surface phase as either a monolayer or multilayer. The literature presents a number of isotherm models. Different isotherm models are used in the current work to describe the equilibrium nature of the adsorption process. To evaluate the suitability of experimental equilibrium adsorption data for CV adsorption onto ACSLS, isotherm models such as Temkin, Freundlich, Langmuir, Redlich-Peterson (R-P), Toth, Radke-Prausnitz, and D-R models were utilized. The equations below (Onal, 2006; Lataye et al., 2009) represent these isotherms. The Langmuir isotherm model assumes sorption of monolayer of sorbate onto a sorbent surface with a finite number of identical sites and the sites equally energetic.

$$\text{Langmuir}, q_e = \frac{q_m b C_e}{1 + b C_e} \text{ or } \frac{C_e}{q_e} = \left(\frac{1}{q_m b}\right) + \frac{C_e}{q_m} \quad (6)$$

$$Redlich - Peterson, q_e = \frac{K_R C_e}{1 + a_R C_e^\beta} \text{ or } ln(K_R \frac{C_e}{q_e} - 1)$$

$$= ln a_R + \beta ln C_e \quad (7)$$

$$Radke - Prausnitz, q_e = \frac{K_{RP} K_{RP} C_e}{1 + K_{RP} C_e^P} \text{ or } \frac{C_e}{q_e} = \frac{1}{K_{RP} k_{rp}} + \frac{C_e^P}{k_{rp}} \quad (8)$$

$$Temkin, q_e = B_T ln K_T + B_T ln C_e \quad (9)$$

$$Toth, q_e = \frac{q_{Th} C_e}{(1/K_{Th} + C_e^{Th})^{1/Th}} \text{ or } \left(\frac{C_e}{q_e}\right)^{Th}$$

$$= \frac{1}{(q_{Th})^{Th} K_{Th}} + \frac{(C_e)^{Th}}{(q^{Th})^{Th}} \quad (10)$$

$$Freundlich, q_e = K_F C_e^{\frac{1}{n}} \text{ or } ln q_e = ln K_F + (1/n) ln C_e \quad (11)$$

Table 1 Influence of dye concentration on its own percentage removal.

Dye concentration (mg/L)	ACSLS		ACR	
	Adsorption percentage (%)	Adsorption capacity (mg/g)	Adsorption percentage (%)	Adsorption capacity (mg/g)
30	97.3	65.9	84.6	54.6
60	92.5	121.2	73.5	93.9
90	87.3	173.1	67.4	132.7
120	74.3	172.8	52.5	130.3

Table 2 Isotherm constants for CV sorption onto ACSLS.

Isotherm Model	Constants	Temperature in Kelvin		
		298 K	308 K	318 K
Langmuir	q_m (mg/g)	204.8	213.5	235.7
	b (L/mg)	3.545	5.867	6.314
	R_L	0.419	0.431	0.525
	R^2	0.998	0.999	0.999
Freundlich	K_F (mg/g)	11.46	13.85	15.21
	N	4.67	6.78	7.13
	$1/n$	0.426	0.317	0.267
	R^2	0.966	0.969	0.968
Temkin	B_T	0.267	0.488	0.521
	K_T (L/mg)	54.678	57.141	75.221
	R^2	0.959	0.956	0.959
Redlich-Peterson	a_R(L/mg)	1	1	1
	K_R(L/mg)	3.827	3.215	3.977
	β	0.971	1.003	1.002
	R^2	0.978	0.979	0.979
Toth	Th	0.843	0.912	0.943
	q_{einf} (mg/g)	2.686	2.474	2.518
	K_{Th} (mg/L)Th	2.599	2.212	2.458
	R^2	0.923	0.936	0.947
Radke-Prausnitz	P	0.872	0.892	0.923
	K_{RP} (L/g)	8.450	4.262	4.462
	K_{rp} (mg/g)/(mg/L)$^{1/P}$	1.531	1.690	1.774
	R^2	0.897	0.887	0.858
D-R	q_m	174.2	184.6	194.7
	E_m (kJ/mol)	24.56	26.23	27.13
	K (mol^2/J^2) $\times 10^3$	4.67	5.12	7.98
	R^2	0.984	0.985	0.987

$$Dubinin - Radushkevich(D-R), \ln q_e = \ln q_m - K\varepsilon^2 \qquad (12)$$

$$\varepsilon = RT \times \ln[1 + (\frac{1}{Ce})] \qquad (13)$$

$$E_m = \frac{1}{\sqrt{2K}} \qquad (14)$$

For adsorbent surfaces with a non-uniform heat of adsorption distribution throughout the surface, the Freundlich isotherm is valid. The Langmuir isotherm, on the other hand, states that sorption occurs uniformly throughout the adsorbent. While the Redlich-Peterson, Toth, and Radke-Prausnitz isotherms can be applied to both homogeneous and heterogeneous systems, the D-R isotherm provides a fair indicator of the physical or chemical nature of adsorption. Table 2 displays the isotherm parameters and correlation coefficients needed to adsorb CV dye onto ACSLS. Using the solver-add-in tool of Excel 2007, nonlinear regression analysis was carried out to determine the isotherm parameters by fitting the experimental data.

When referring to the affinity of the accessible sites and the free energy of sorption, the Langmuir constant b (L/mg) is used. q_e stands for dye concentration onto sorbent at equilibrium (mg/g). C_e is the dye's equilibrium concentration in solution (mg/L) q_m in mg/g symbolizes maximum capacity of adsorption based upon Langmuir model. When the sorbent is covered by a monolayer, the dye concentration is q_{max} (mg/g). Drawing C_e/q_e vs C_e yielded values for the Langmuir correlation coefficient R^2 that ranged from 0.988 to 0.999 (Table 2) for the temperature range of 298 to 318 K, indicating

that the isotherm model is highly appropriate for the experimental data (Fig. 5a). Table 2 provides a list of all model parameters. The isotherm model's applicability was also examined using R_L. R_L can be determined using equation (15) as mentioned below (Lataye et al., 2009):

$$R_L = \frac{1}{1 + bC_0} \qquad (15)$$

Where, starting concentration for dye is represented as C_0. R_L value is a crucial factor for Langmuir isotherm as it helps in revealing the nature of sorption process in terms of its favourability for forward or backward sorption. If $R_L = 1$, it implies sorption process is proportionate, R_L greater than 1 will suggest sorption is not feasible, if condition is $0 < R_L$ less than 1, it indicates favourability of the sorption process and if $R_L = 1$, sorption process is supposed to be irreversible. For the present study, R_L values for the given range of temperature were found out to be as 0.219–0.325 indicating favourability for adsorption of CV onto anionic surfactant modified adsorbent. Theoretical maximum adsorption capacities for ACSLS and ACR for the given case was found out to be as 237.6 mg/g and 138.5 mg/g respectively.

For the Freundlich model, the constants K_F and $1/n$, respectively, show the adsorption capacity and intensity. The value of $1/n$ increases with the degree of heterogeneity and bonding between the adsorbent sites and the adsorbate. Table 2 demonstrates that K_F values increase with increasing temperature, implying that ACSLS absorbs more dye at higher temperatures and demonstrating the endothermic nature of the adsorption process. The type and potency of the adsorp-
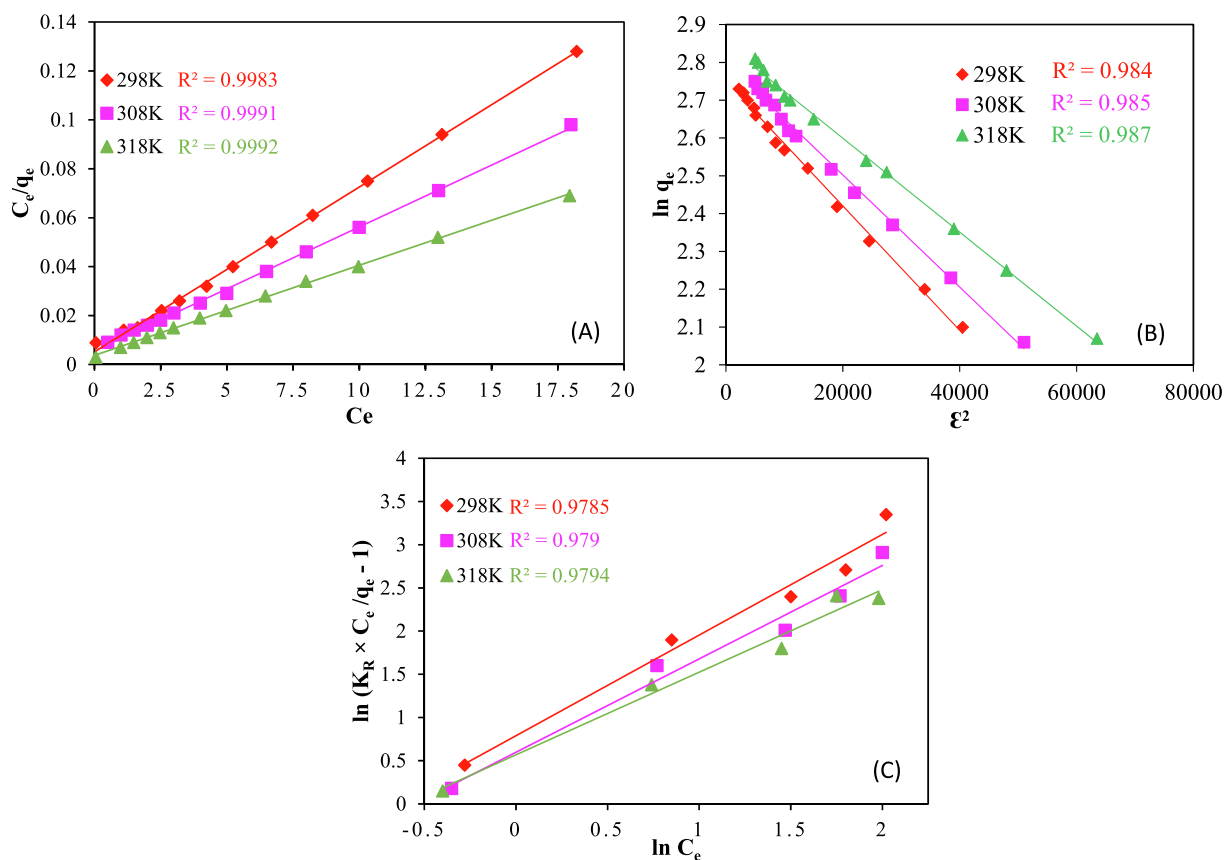
Fig. 5 Plot for **(a)** Langmuir isotherm **(b)** D-R isotherm and **(c)** Redlich-Peterson isotherm for CV removal onto ACSLS (adsorbent dose = 100 mg/L, pH = 6.0, C_0 = 30–90 mg/L).

tion process determines how the $1/n$ numbers, which indicate the relative distribution of energy sites, behave. Given that $1/n = 1$, ACSLS preferentially absorbs CV dye at all temperatures. The Temkin constant and the heat of dye adsorption onto ACSLS are related (B_T). Under every condition, B_T rises as the temperature rises. Temkin's model presents the chemical interactions between the adsorbent and adsorbate using a constant K_T. Three parametric Redlich-Peterson models may effectively explain both uniform and non-uniform systems of adsorption interaction. The viability of the adsorption process is implied if the value is between 0 and 1. The isotherm exponent Th for the Toth model, which typically comes out to be smaller than unity, accounts for the heterogeneity of the sorption system. When the exponent value deviates from unity, it will be apparent that the sorption is not uniform. When the exponent value merges with one, the Toth isotherm becomes the Langmuir model. When the P value for the model reaches one, the Radke-Prausnitz model will also imply the Langmuir model. For Redlich-peterson model, β in the proximity of 1 indicates favourable adsorption at higher temperatures, with the exception of 298 K. Adsorptions can be divided into three categories based on their mean free energy value, E_m: If the E_m value is less than 8 KJ/mol, physical adsorption will be used to manage the adsorption process. (ii) If E_m value is between 8 and 16 KJ/mol, ion exchange will promote the adsorption process, and (iii) if E_m value is between 16 and 400 KJ/mol, chemical adsorption will be the main controlling factor. E_m values for the current example were discovered to be 24.56, 26.23,

and 27.13 KJ/mol respectively, for corresponding temperatures of 298, 308 and 318 K, supporting chemisorption.

The experimental data at the equilibrium point suit the Langmuir model the best, followed by the D-R and Redlich-Peterson models, according to analysis of isotherm models. The Langmuir model's suitability showed that CV sorption was uniform across the adsorbent surface. According to the findings, anionic surfactant treatment of AC caused a constant pore distribution over the AC surface, aiding in the uniform and homogenous adsorption of CV dye. It may be deduced from the analysis of kinetics (discussed later) and isotherms that sorbent and sorbate's adsorptive interaction led to monolayer chemical adsorption.

3.8. Analysis of error function

In order to choose the best fit model, a large amount of data from the examination of dye adsorption by surfactant modified AC (ACSLS) was analysed on numerous linearized models. However, because of the inherent bias caused by linearization, non-linear regression equations were used to establish sets of various isotherm parameters. This provides a mathematical method for determining the isotherm's parameters using the real isotherm equation. In order to match the experimental equilibrium data to the isotherm data, the optimization strategy needs an error function. The data fits into a zone of high concentration because the error function selected affects the parameters of the derived-error function,

which is mostly dependent on absolute deviation bias. When extreme errors are penalized by the square of the deviation, this weighting is raised even further. To show the value of fractional deviation, the bias can be offset by dividing the deviation with the aid of a computed value. By minimising the different error functions over the concentration range and using Solver add-in with Microsoft Excel, isotherm parameters were found during the study of error function isotherms. The initialization of this programme is based on a clever guess parameter. Using the data received from the linearized version of the model, an iterative operation was initiated in Microsoft Excel. The numerous error functions are described in the sections as follows.

3.8.1. The sum of the absolute errors (SAEs)

The summation of the method of absolute errors can be given by the following equation:

$$SAE = \sum_{i=1}^{n} |q_{e,exp} - q_{e,cal}| \tag{16}$$

Where $q_{e,exp}$ is the adsorbate concentration that was adsorbed during the experiment, which was calculated from the concentration of equilibrium sorbate liquid phase, C_e was achieved experimentally, and $q_{e,cal}$ is the concentration of theoretical solid phase of sorbate that was adsorbed onto the sorbent, which was calculated using one of the isotherm equations. The data of the error function is raised by biassing the fit towards the zone of high concentration, which is done by using error functions to determine isotherm parameters.

3.8.2. The sum of the square of the errors (SSEs)

The summation of the squares of the error's method can be written as follows:

$$SSE = \sum_{i=1}^{n} (q_{e,cal} - q_{e,exp})_i^2 \tag{17}$$

The isotherm parameters that are computed using this error function provide a better fit as the error value, hence the biassing of fit towards data acquired at the high end of the concentration range increases as the square of the magnitude of error increases. Despite being the most often used error function, the error function has a number of drawbacks.

3.8.3. The hybrid fractional error function (HYBRID)

The sum of the square of the error is divided by the measured value to best suit the sum of the square of the error at a very low concentration. Porter et al. created an error function to achieve this better match. It also uses the number of data points minus the number of parameters (n-p) and the number of degrees of freedom of the system as a divisor in the isotherm equation. It is written as follows:

$$HYBRID = \frac{100}{n - p} \sum_{i=1}^{n} \left[\frac{q_{e,exp} - q_{e,cal}}{q_{e,exp}} \right]_i \tag{18}$$

3.8.4. Marquardt's percent standard deviation (MPSD)

It is represented as:

$$MPSD = 100 \sqrt{\left(\frac{1}{n - p \{ \sum_{i=1}^{n} \left(\frac{q_{e,exp} - q_{e,cal}}{q_{e,exp}} \right)_i^2 \}} \right)} \tag{19}$$

This error function is used by different researcher in this subject in the past. It sometimes resembles the geometric mean error distribution, which improves with the number of degrees of freedom of the system (Lataye et al., 2011).

3.8.5. Average relative error (ARE)

The average relative error function (Marquardt, 1963) is:

$$ARE = \frac{100}{n} \sum_{i=1}^{n} \left[\frac{q_{e,exp} - q_{e,cal}}{q_{e,exp}} \right]_i \tag{20}$$

This error function tries to keep the fractional error distribution as small as possible throughout the whole concentration range.

3.8.6. Chi-square ($\chi 2$) test

$$\chi 2 = \frac{(q_{e,exp} - q_{e,cal})^2}{q_{e,cal}} \tag{21}$$

The sum of square of difference between actual experimental data and theoretical data predicted from using various models is defined as Chi-square with all the individual difference of square being divided from each respective data produced from models. When comparing the fitness of isotherms, the lowest values of χ^2 are used in error analysis and the greatest values of R^2 are used when evaluating the fitness of isotherms. Study of error analysis revealed that among all the models, hybrid fractional error study explores lowest error distribution of the experimental data. Error analysis values for several models are presented using table S3.

From the inference of results of the error functions values (Table S3) and the values of coefficient of correlation for the isotherms (Table 2), the suitability of isotherms for the present study is found in the following order: Langmuir > D-R > Redlich-Peterson > Radke − Prausnitz > Toth > Temkin > Freundlich.

As per the fitness, three of the best-fit isotherms (Langmuir, D-R and Redlich-Peterson) are shown using 5 (a), (b) and (c) respectively. For Langmuir model, the curve is plotted between C_e/q_e and C_e, for D − R model, the curve plotted between $\ln q_e$ and $\mathcal{E}^2$ and Redlich-Peterson is plotted using $Ln (C_e)$ and $Ln (K_R \times C_e/q_e − 1)$.

3.9. Effect of temperature and thermodynamics parameters

Fig. 6a shows the findings of an investigation into three separate CV dye concentrations (30, 60, and 90 mg/L) at various temperatures (298 K, 308 K, and 318 K). The capacity of CV to adsorb onto ACSLS was inversely correlated with concentration and directly proportional to temperature increase. This demonstrated that the adsorption was an endothermic, spontaneous process. The chemical potential, solubility, and thermal motion of dye molecules all increased with temperature (Kapoor and Yang, 1989). Furthermore, it was discovered that the AC's pore structure and temperature have a strong correlation. Because of thermal expansion, as temperature increased, activated carbon's pore structure and active adsorption sites increased as well. These considerations have caused the capacity of CV to adsorb on ACSLS to rise with temperature.
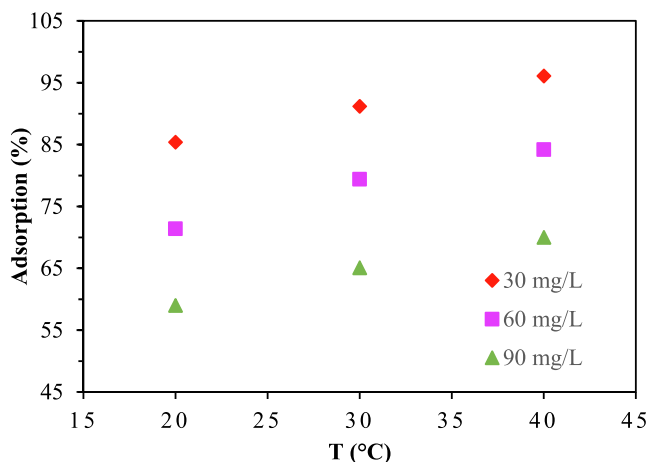
Fig. 6a Effect of Temperature variation on CV removal onto ACSLS (Sorbent dose = 100 mg/L, Time = 120 min, pH = 6.0).

Fig. 6b Van't Hoff's plot for CV sorption onto ACSLS.

The influence of temperature and the mechanism of sorption were further examined in the research of adsorption thermodynamics. The thermodynamics of ACSLS adsorption were looked into from an energy perspective. The driving force of adsorption and whether or not the adsorption process was spontaneous were both investigated using the adsorption thermodynamics approach. The thermodynamic formulae provided in equations are used to evaluate the changes in enthalpy (ΔH), free energy (ΔG), and entropy (ΔS) (22) – (25) (Mouni et al., 2018):

$$\Delta G = -RTlnK_C \tag{22}$$

$$K_C = \frac{q_e}{C_e} \tag{23}$$

$$\ln K_C = \frac{\Delta S}{R} - \frac{\Delta H}{RT} \tag{24}$$

$$\Delta G = \Delta H - T\Delta S \tag{25}$$

Where, T is temperature in Kelvin (K), universal gas constant is represented as R (8.314 J/mol/K), and K_C is the thermodynamic constant. Change in Gibbs free energy (kJ/mol), change in entropy (kJ/mol/K), and change in enthalpy (kJ/mol) are all represented by the letters ΔG, ΔS, and ΔH respectively. Parameters of Van 't Hoff's graph for ln K_C vs $1/T$ is depicted using Fig. 6b and is used to calculate ΔH and ΔS values, which are presented using Table S4.

The negative ΔG values demonstrated by Table S4 demonstrated the applicability and spontaneity of the CV sorption process on ACSLS (Gobi et al., 2011). The decrease in ΔG values with increasing temperature shows that the adsorption process is more favourable at high temperatures. Positive ΔH values of 9.67, 14.89 and 16.22 KJ/mol at rising temperatures at initial dye concentrations of 30, 60, and 90 mg/L, respectively, demonstrate that the adsorption process was endothermic (Auta, 2014). The values were obtained for the adsorption of various CV dye concentrations on ACSLS for the change in entropy (ΔS) are 0.071, 0.085, and 0.089 kJ/mol/K. Positive values of ΔS (Bulut and Aydın, 2006) represented the increased sorption arbitrariness during solution and solid interaction.
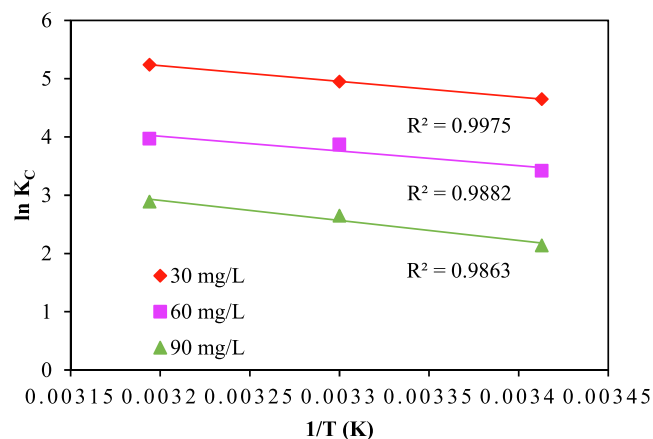
3.10. Activation energy analysis

When an adsorbate particle collides with the surface of an adsorbent with a particular minimum energy and a particular direction, adsorption occurs. Adsorption cannot take place unless the adsorbate particle can cross the energy wall that is on the surface of the adsorbent. The bare minimal amount of energy necessary for the adsorption process is called activation energy. Physical adsorption controls the adsorption process if the activation energy is less than 40 kJ/mol, while chemical adsorption is preferred if it is greater than 40 kJ/mol (Anirudhan and Radhakrishnan, 2008). Using the Arrhenius equation, the activation energy of the process is determined as follows:

$$K_{p2} = Ae^{-E_a/RT} \tag{26}$$

Where, K = Adsorption rate constant, R = Ideal gas constant, A = Constant of proportionality which vary from one process to another, E_a = Activation energy of the process, T = Temperature (Kelvin).

Applying operation of natural log (at the base e) on both the side of equation (26) gives the linearized form of the Arrhenius relation as:

$$\ln K_{p2} = \ln A - \frac{E_a}{RT} \tag{27}$$

By plotting the curve (figure S9) of ln K_{p2} versus $1/T$, we were able to estimate the activation energy of our adsorption system. In relation to equation (27), (- Ea/R) value is determined from the slope of the straight line derived from the linearized form of the Arrhenius equation. The maximum E_a value was calculated to be 45.36 KJ/mol, indicating that the current study favoured chemical adsorption.

3.11. Study of kinetics

3.11.1. Intra-particle diffusion/pore diffusion model and film diffusion model

The equation proposed by Weber & Morris gives the rate limiting step in pore diffusion-.

$$q = K_{id}t^{1/2} + C_i \tag{28}$$

Where, q denotes the amount of adsorbate adsorbed in mg/g at time t and K_{id} denotes the intra particle rate constant.

Equation presented using eqn. (6) is the form of straight-line $y = mx + c$; Where $y = q$, $x = t^{\frac{1}{2}}$, slope $m = K_{id}$ and Y-intercept $= C_i$,

The C_i value establishes the boundary layer effect's thickness. The influence of the boundary layer will be stronger the larger the magnitude of the intercept. Only pore diffusion is thought to be the rate-regulating step if the line departs from the origin. The results of the pore diffusion investigation for removing CVs using ACSLS are given in Fig. 7b, which shows experimental data fitted for pore/intra particle diffusion, shows that the linear line of the plot does not pass through the origin, suggesting that intra particle diffusion was not the only process controlling the sorption process and that additional processes were also involved in the mass transfer process. The fact that the intercept constant C_i (83.4, 101.9, 117.7) rose as the sorption advanced as the CV dye concentration suggests that the boundary layer thickness may have increased as the sorption advanced (refer Table 3). For all dye concentrations, high intercept constant values indicated that film diffusion also played a significant role in the early stages of the sorption process. However, strong correlations (0.9–0.95) revealed that intra-particle diffusion also had an impact. Another figure S10 shows the relationship between the amount of CV dye that

can be adsorbed onto the ACSLS at time t and the amount of CV dye that is present in the solid phase at time t (square root of time) at 298 K to better illustrate intra particle diffusion. Two separate linear lines that do not overlap at the origin make up the whole plot in figure S10. The amplitude of the intercept value for the straight line also rose from the origin as the contact time increased, showing a thickening of the boundary layer and, consequently, an increase in the effect of film diffusion, which also contributed to the adsorption process.

Adsorbate diffusion to the adsorbent surface from the liquid phase is a crucial point to be considered in obtaining the rate of adsorption. The liquid film diffusion model was proposed by Byod as follows:

$$\ln(1 - F) = -k_{fd}t \qquad (29)$$

Where $F = q_t/q_e =$ fractional attainment of equilibrium.

In the Boyd plot, a graph is plotted between $\ln \left(1 - \frac{q_t}{q_e}\right)$ versus t. Film diffusion is symbolised if the graph is in linear form and passes through the origin and is represented as the slowest (rate-controlling) step in the adsorption process. This approach/model has limited relevance if the graph does not travel via the origin. The findings of the film diffusion study for CV sorption onto ACSLS are shown in figure S11. As per analysis, the linear plot for film diffusion also do not pass
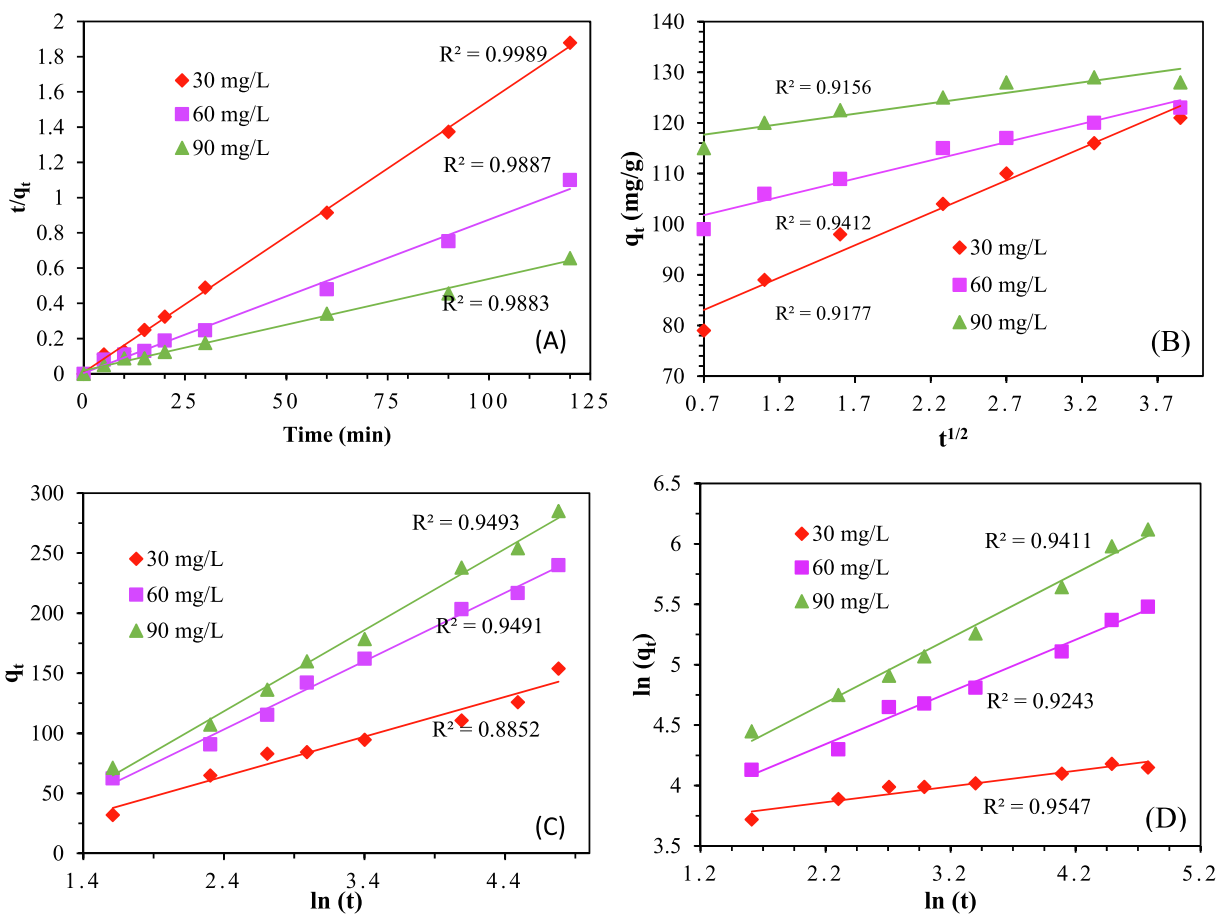
Fig. 7 Plot for **(a)** Pseudo 2nd order rate kinetic **(b)** Intra Particle diffusion model **(c)** Elovich model and **(d)** Modified Freundlich model (pH = 6.0, adsorbent dose = 100 mg/L, Time = 120 mins).

through the origin, but close to origin showing that film diffusion also has part in the absorption analysis. Likewise other kinetic models are discussed as below.

3.11.2. Pseudo 1st and 2nd order kinetic study

Pseudo 1st order model can be expressed as (Eren and Acar, 2006):

$$\frac{dq}{dt} = K_f(q_e - q_t) \qquad (30)$$

In the above, K_f = equation for Pseudo 1st order constant, q_e = Equilibrium sorption capacity in mg/g, q_t = sorption capacity at any given time t, t = time in minutes. Integrating equation (30) and equating to C_0 = 0 at t = 0 we get:

$$\log(q_e - q_t) = K_f(q_e - q_t) \qquad (31)$$

Also, equation for 2nd order rate model can be expressed as (Lagergren, 1898):

$$\frac{dq}{dt} = K_s(q_e - q_t)^2 \qquad (32)$$

Where, K_s = constant for rate of reaction (g/mg min).

Second order rate kinetic is understood to be proportionate for concentrations equivalent to two reactants, and also this rate kinetic symbolizes chemical sorption and hence fast and high sorption. Now integrating equation (10) and using q_t = 0 and time, t = 0, new form of equation (33) can be expressed as:

$$\frac{t}{q_t} = \frac{1}{K_S q_e^2} + \frac{1}{q_e} t \qquad (33)$$

Where, $K_S q_e^2$ is the sorption rate h at stating stage with time, t = 0.

The important kinetic equation parameters, which were determined from the slopes and intercepts of the linear plots (refer Fig. 7a), are shown in Table 3. The correlation coefficient values show that the pseudo 1st order model has a better fitness than the pseudo 1st order model. Additionally, it can be seen that the 1st order rate kinetic values differ significantly from the experimental data while the 2nd order kinetic values are consistent with the experimental values, supporting the suitability of the pseudo 2nd order rate kinetic model. This is demonstrated by comparing the adsorption capacity data from experiments with the adsorption capacity calculated using models. There is no trend for K_f values for Pseudo 1st order, as seen in Table 3. Analysis revealed that K_s values dropped in line with rising dye concentration. As a result, the rate of adsorption decreases as the concentration of solute rises, which is consistent with other observations using different adsorbents (Ho and McKay, 1999; Ho et al., 2005; Dey et al., 2022; Bansiwal et al., 2009).

3.11.3. Elovich model and modified Freundlich model

The equation for Elovich can be represented as (Dey et al., 2022; Onal, 2006).

$$\frac{dq_t}{dt} = \alpha e^{-\beta t} \qquad (34)$$

In the above,

α = rate at starting stages (mg/g/min) and β (g/mg) is corelated to the limit of surface coverage and activation energy for chemisorption.

Table 3 Kinetic constants for CV sorption onto ACSLS.

Model Constants	Concentration (mg/L)		
	30	60	90
	$q_{e,\ exp}$ (mg/g)		
	127.7	194.5	236.4
Pseudo 1st order			
$q_{e,\ calc}$ (mg/g)	32.7	99.5	142.8
K_f(min^{-1})	0.0076	0.049	0.0068
R^2(linear)	0.833	0.886	0.917
Pseudo 2nd order			
$q_{e,\ calc}$ (mg/g)	108.6	173.4	214.8
h(mg/g/min)	1.321	1.355	1.739
K_s(min^{-1})	0.493	0.436	0.371
R^2(linear)	0.998	0.988	0.988
Elovich model			
β (g/mg)	7.278	4.872	6.671
α (mg/g/min)	8.78×10^5	0.587	3.54×10^8
t_0	1.012×10^{-5}	1.172	3.325×10^{-8}
R^2(linear)	0.885	0.949	0.949
Modified Freundlich			
m	0.437	0.361	0.253
k (dm^3/g/min)	0.476	0.167	0.384
R^2 (linear)	0.954	0.924	0.941
Intra Particle Diffusion			
K_{ip}	3.78	4.56	4.89
C_i	83.5	102	117.5
R^2	0.917	0.941	0.915

Equation describing straight line can be given as below:

$$q_t = \frac{1}{\beta}\ln(\alpha\beta) + \frac{1}{\beta}\ln(t) \tag{35}$$

The Elovich equation's constants are determined from the plot of $\ln(t)$ versus qt (Fig. 7c). Apart from Pseudo 1st order and 2nd order, Elovich constants are also listed using Table 3.

The equation of modified Freundlich was actually given by Kuo and Lotse (1973). It can be represented as:

$$q_t = kC_0t^{1/m} \tag{36}$$

In the above, m = constant given by Kuo and Lotse, rate constant for apparent sorption, q_t = sorption capacity at any given time, t in mg/g, C_0 = starting dye concentration in mg/L. When simplified, modified Freundlich model can be written in the form of straight line as:

$$\ln q_t = \ln(kC_0) + \frac{1}{m}\ln t \tag{37}$$

The constants are determined from the graph of $\ln qt$ versus $\ln t$, as shown in Fig. 7d. Along with other kinetic constants, all the modified Freundlich model constants are given in Table 3.

From the analysis of kinetics, it was revealed that experimental data fitted best with the Pseudo 2nd order rate kinetic for adsorption of CV dye onto surfactant modified AC and thus also suggesting that process was favoured by chemisorption. Studies suggested that sorption mechanism wasn't entirely supported by the combination of intra particle and film diffusion at different stages of process but also controlled by 2nd order rate kinetic where electrons were transferred between cationic and anionic functional groups present in the CV dye and surfactant modified AC surface.

3.12. Isosteric heat of adsorption

The adsorption heat at a constant surface coverage is known as the isosteric heat i.e., at a particular constant quantity of adsorbate material that has been adsorbed at the adsorbent surface and it is calculated using the integrated Clausius-Clapeyron equation:

$$ln Ce = (-\Delta Hx/R)1/T + \text{constant} \tag{38}$$

At equilibrium, Ce (mg/L), denotes adsorbate concentration, ΔHx denotes the isosteric heat of adsorption (kJ/mol), R refers the ideal gas constant (8.314 J/mol/K), and T is temperature (Kelvin scale). The adsorption isostere in the form of a straight line is obtained in equation (38) and the value of ($-\Delta Hx/R$)is obtained from slope of the straight line between Ce vs $1/T$. For constant surface loading (SL), the best fitted isotherm model gives the value of Ce. For SL of constant rate, C_e values were obtained from the best fitted isotherm model as per section 3.7 of this article. Accordingly, C_e values were calculated from the Langmuir isotherm for the process and were considered for isosteric heat analysis. Study was conducted for four different surface loadings viz. 10, 12, 14 and 16 mg/g at 298 K, 308 K and 318 K. Result for the same is shown using Fig. 8a.

The isosteric heat of adsorption is primarily dependent on temperature and SL. If the isosteric heat increases as the temperature rises, the process is said to be endothermic. Similar to this, something is considered to be exothermic if the isosteric heat drops as the temperature rises. The isosteric heat of adsorption will be constant and independent of surface loading if the adsorbent surface is uniform. The surface of the adsorbent is energetically heterogeneous, which favours adsorption, if the isosteric heat of adsorption, however, fluctuates with surface loading. It is also demonstrating the existence of potent lateral interactions between molecules that have been adsorbed. The predominance of adsorbate–adsorbate interaction leads to the low value of isosteric heat of adsorption, whereas the predominance of adsorbent-adsorbate interaction leads to the high value of isosteric heat of adsorption. Fig. 8b depicts the rise in isosteric heat as a function of temperature, indicating that the adsorption was endothermic in nature, which is consistent with the thermodynamic analyses conducted for this work.

3.13. Column study

In order to operate at higher throughput, industrial scale operations attempt to attain the highest flow rate possible. A glass column measuring 2 cm in diameter and 50 cm in length was used to analyze the performance of the adsorbent column. Glass wool was placed at the bottom of the column to provide support for the adsorbent before 2 g of ACSLS with a 10 cm
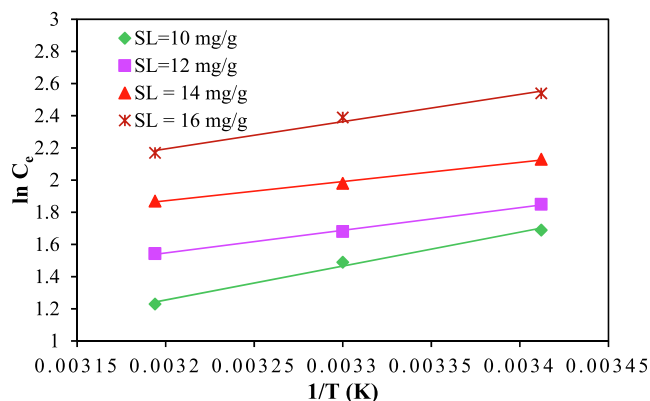

Fig. 8a Relation between ln (C_e) vs $1/T$ for CV adsorption onto ACSLS.
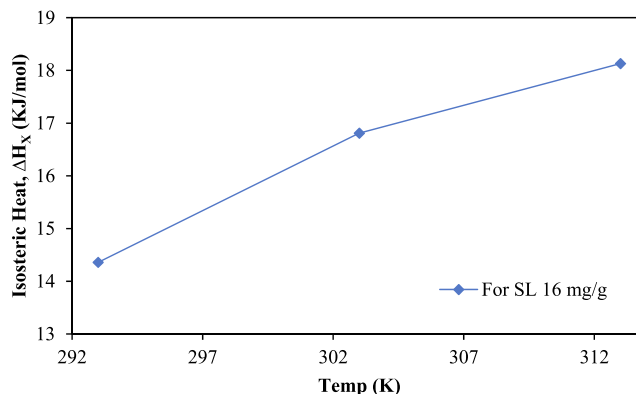

Fig. 8b Plot between ΔH_X vs Temperature (K) for sorption of CV onto ACSLS.

initial bed depth was added. A 25 mg/L CV solution was passed through the column at flow rates of 0.5, 1.0, and 1.5 mL/min. The cleaned water was gathered and placed in a conical flask. The experimental break through curves (S-curves) generated for various flow rates are shown in Figure S12a. Shorter contact times resulted in larger flow rates and early breakthrough. The adsorption capacity rises at low flow rates up to 0.5 mL/min but decreases as the flow rate rises from 0.5 to 1.5 mL/min due to insufficient contact time. Since 0.5 mL/min flow rate demonstrated the greatest adsorption, this flow speed and bed depth of 10 cm were used for the column investigation utilizing a range of dye concentrations, including 25, 50 and 75 mg/L. The findings are shown in figure S12b. In comparison to the other two concentration trials (25 and 50 mg/L), analysis showed that adsorption with a greater concentration (75 mg/L) achieved early breakthrough. Similar research has been conducted using three different bed depths of 10, 20, and 30 cm with constant flow rates and dye concentrations of 0.5 mL/min and 25 mg/L, respectively. Figure S12c uses the results of column analysis utilizing bed depth variation.

To characterize the fixed bed column behaviour and scale it up for industrial applications, several ground-breaking models, including the Thomas, Yoon-Nelson, Bohart-Adam, and Clark models, were used for different flow rates to match the experimental results of the column investigations. Each of these models is distinct from the others in terms of the column adsorption isotherm, the inclusiveness or exclusivity of reactions, significance, and the type of rate law used (Goswami and Dey, 2022; Ghasemi et al., 2011).

A general model for analyzing column performance when both the exterior and interior diffusion resistances are extremely low is the Thomas model. In this model, it is anticipated that the adsorption behaviour will follow second-order reversible reaction kinetics and a Langmuir isotherm without axial dispersion.

Linear form:

$$\ln(C_e/C_0 - 1) = k_{TH}q_0m/Q - k_{TH}C_0t \tag{39}$$

Yoon and Nelson devised a simpler model that requires no precise information on the adsorbate's characteristics, the adsorption bed's parameters, or the kind of adsorbent. The rate of decline in the likelihood of an adsorbate molecule is considered to be proportional to the probability of adsorbate adsorption and the probability of an adsorbate breakthrough on the adsorbent in this model.

Linear form:

$$\ln[C_e/(C_0 - C_e)] = k_{YN}t - k_{YN}\tau) \tag{40}$$

The equilibrium, according to Bohart-Adams, is not immediate. The adsorption capacity depends on the adsorbent, and adsorbing species concentrations are proportional to adsorption rate.

Linear Form:

$$\ln\left(C_e/C_0 = k_{AB}C_0t - \left[\frac{kN_0H}{v}\right]\right) \tag{41}$$

The Clark model is based on the usage of the Freundlich isotherm in conjunction with a mass-transfer notion. The Clark model implies that the mass transfer zone's shape remains constant and that all adsorbate is eliminated at the column's end.

Linear form:

$$\ln(C_0/C_e)^{n-1} - 1 = A \times e^{-rt} \tag{42}$$

$$A = \exp(K_C N_0 Z/v)$$

$$r = K_c C_0$$

Fig. 9 shows fitness of various breakthrough curves for varying flow rates with the models. Table S6 results reveal that Thomas model fit better with the experimental data well and had a high R^2 value. Table S6 analytical results indicated that when flow rate increases, k_{Th} and K_C rise, but k_{AB} and k_{YN} drop. The performance of ACSLS as a result of CV dye adsorption follows second order reversible reaction kinetics. (Goswami and Dey, 2022).

3.14. Regeneration studies

Used ACSLS was recycled using effluents like diluted HCl and diluted NaOH. All of the investigations on reusability were conducted at room temperature. Fig. 10a and table S7 depict the desorption and reuse of ACSLS with 1.0 M NaOH at $C_0 = 10$ mg/L for six regeneration cycles, with a capacity of adsorption decreasing from 94.5 % to 49.9 %. Fig. 10b and table S8 present data for desorption with various NaOH concentrations and HCl concentrations (0.2–1.0 M). The best removal efficiency for reuse was attained after desorption using 1.0 M HCl solution, however a concentration that was too high (1.5 M) was unfavorable to reuse, presumably due to residual acidic influence on the ACSLS or adsorbent structural deterioration. Therefore, 1.0 M was chosen as the optimal HCl solution concentration for regeneration.

3.15. Analysis of chemical oxygen demand (COD)

In order to determine the chemical oxygen demand, the digesting system was turned on and a temperature of 150 °C was set (COD). Following that, 10 digestion tubes were chosen, and 50 mL of sample (dye solution with a concentration of 50 mg/L) was placed into each of the tubes. They were added along with normal $K_2CR_2O_7$ and mercuric sulphate (potassium dichromate, strength 0.125 N). The tubes were then placed in a plastic tray, allowed to cool, and then 50 mL of the sulphuric acid reagent were added. The reagent containing sulfuric acid was gradually added. The mixture was then well-combined. The mixture was combined, and the tubes were then kept in a COD digester. The tubes were filled with the air condensers, and the mixture's flow rate was set for 90 min. The COD digester was then allowed to cool to room temperature after the air condensers and tubes from the COD digestion were removed. The COD value was determined by titrating against 0.1 M Ferrous Ammonium Sulphate solution while using 1–2 drops of Ferroin indicator (Assam state pollution control board manual). Using a COD block digesting system, the test was run (model Pelican Kelplus- 08LCAC). Following is how the COD value (in mg/L) was calculated.:

$$COD\,(mg/L) = ((blank - sample) \times 0.1$$
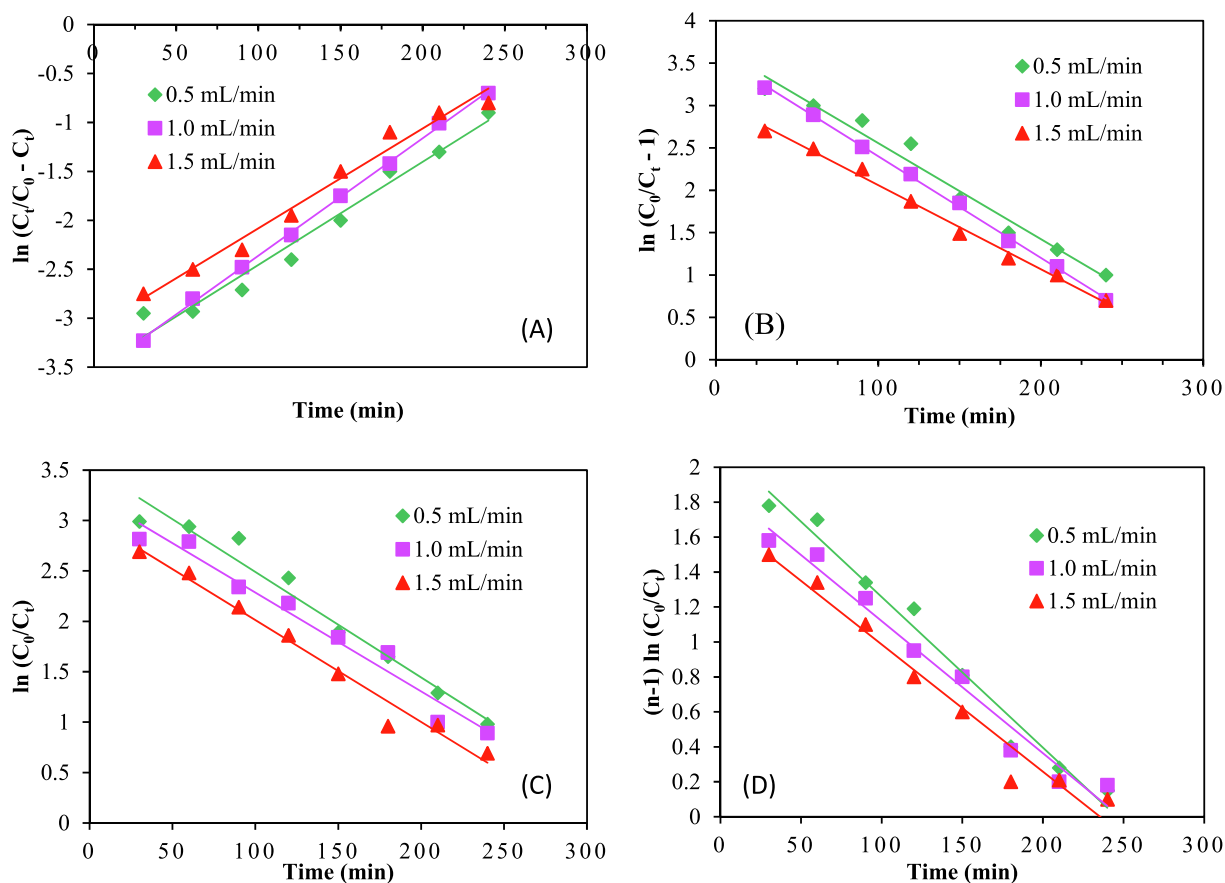$$\times\, 8000)/(volume\,of\,sample) \tag{43}$$

Fig. 9 Breakthrough curves for: **(a)** Yoon − Nelson model **(b)** Thomas model **(c)** Bohart − Adam model and **(d)** Clark model.
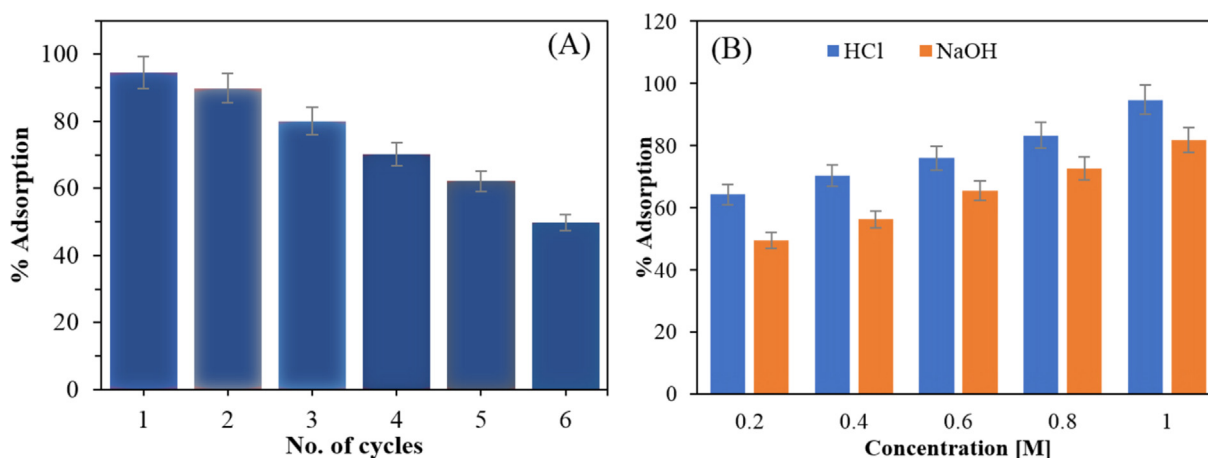

Fig. 10 **(a)** Adsorption-regeneration cycle **(b)** Regeneration of ACSLS with NaOH and HCl.

According to observations (data not provided), the sample solution's COD value was 134.82 mg/L before adsorption and decreased to 56.23 mg/L after. Therefore, it is evident that the COD value of the water solution was higher prior to adsorption due to the presence of higher initial concentrations of CV dye, and as the solution was subjected to adsorption, dye concentration of the solution decreased and ultimately the COD value of the solution came down. Additionally, it shows that any increase in the solution's COD value caused by the addition of ACSLS was minimal, suggesting that the substance was stable in water solution and did not release any chemicals into the mixture during the adsorption process. The reduced COD value of the solution after the adsorption process and the removal of dye indicates the fitness of the ACSLS as an efficient adsorbent for the removal of CV dye from the solution.

3.16. Influence of additive salts and coexisting anions

For the investigation of influence of various salts such as $MgSO_4$, $FeSO_4$, KCl, $CaCl_2$, $NaNO_2$, NaCl and NH_4Cl 100 mL of CV solution was used for each of the dye concentration values viz. 30, 60 and 90 mg/L. After adjusting the solution pH at 6.0 and oscillation of 30 min, tests were carried by adding 100 mL of additive salts in the dye solution for each salt compound. Influence of salts on sorption capacity is illustrated using Table 4.

The adsorption of CV onto ACSLS was little affected due to coexistence of ions/salts in the solution mix. The dye removal rates were 79.1 % − 83.1 % for 60 mg/L dye concentration, in the presence of coexisting ions, and it was found more or less same to removal rates of 82.3 % when the ions were absent. For 90 mg/L initial CV concentration, the clearance rate of CV in the presence of coexisting ions (54.4 % − 57.5 %) was similar to when ions were absent (56.9 %). This finding is comparable to other work on the influence of cations on ammonium adsorption on ACSLS (Yagub et al., 2012). It showed that the adsorption mechanism was unaffected by ionic species such as NH^{4+}, Na^+, Ca^{2+}, K^+, and Mg^{2+}.

The capacity of adsorption of CV onto ACSLS in presence of NaCl, $CaCl_2$, or NH_4Cl increased marginally. This can be attributed to the enhanced deionization method of CV dye in aqueous mix due to dipole–dipole interaction, ion dipole forces and van-der-Waals interaction bonding between molecules of dye. Previous findings also reported that additional minerals/salts increase the dye removal rate by AC carbon subjected to surfactant modification (Abdel-Fattah et al., 2015). Pres-

ence of (NO^{2-}) ion had a stronger influence on the adsorption of CV by ACSLS. For NO^{2-} presence in aqueous mix, CV removal rate is reported as 85.8 % which is higher when compared to absence of same ion when the CV concentration was 60 mg/L (for solution in absence of NO^{2-} removal = 82.3 %). It's possible that this is because NO^{2-} has a high oxidation capacity in dilute solutions. In dye manufacturing, nitrites such as potassium and sodium nitrite are commonly employed. When experiments were carried for 90 mg/L, removal rate of CV (48.5 %) by ACSLS during presence of (Fe^{2+}) was recorded to be lesser when compared with absence of the particular ion (56.9 %). Adsorption rate deteriorated as ferrous ions with high sorption reducibility filled the CV adsorption site on ACSLS.

3.17. Adsorption of CV onto ACSLS using real water samples

The CV adsorption rate onto ACSLS for three different water samples—tap water, natural water, and waste water—is shown in Table S9. Water samples were gathered from lab faucets, the Gaurang River in Kokrajhar, Assam, India for the natural water sample, and an unidentified drain on the CITK campus for the waste water sample. A predetermined amount of CV was added to 100. All of the samples were adjusted to a pH of 6.0 and shaken for 30 min to obtain concentrations of 30, 60 and 90 mg/L, respectively. Comparing the results with distilled water samples, the rate of CV adsorption by ACSLS in actual water samples was only slightly higher than it was for modelled dye waste water.

Table 4 Influence of additive salts on CV removal onto ACSLS (Time = 30 min, pH = 6.0).

Dye Conc. (mg/L)	Influence of ion/salts on dye removal (%)							
	$CaCl_2$	KCl	NH_4Cl	NaCl	$NaNO_2$	$MgSO_4$	$FeSO_4$	Without ion/salt
30	96.4	96.4	96.4	96.4	96.4	96.4	92.1	95.7
60	82.7	80.6	81.5	83.1	85.8	79.1	66.2	82.3
90	55.8	55.9	57.2	57.5	59.1	54.4	48.5	56.9

Table 5 Langmuir q_e values for CV dye adsorption using different adsorbents.

Adsorbent	Langmuir q_e (mg/g) CV dye	Reference
SDS modified magnetic Nanoparticles	166.6	(Muthukumaran et al., 2016)
Charred rice husk	62.85	(Homagai et al., 2022)
Xanthated rice husk	90.02	(Homagai et al., 2022)
Treated sugarcane bagasse	107.5	(Omer et al., 2022)
Modified almond shell	12.2	(Loulidi et al., 2020)
Carboxylic group treated activated carbon	120	(Gohr et al., 2022)
Ricinus communis pericarp carbon	48	(Madhavakrishnan et al., 2009)
Magnetite alginate	37.5	(Elwakeel et al., 2017)
Polyvinyl alcohol/agar/maltodextrin	19.17	(Hoang et al., 2020)
Soil-silver nanocomposite	1.918	(Satapathy and Das, 2014)
NaOH-modified rice husk	44.87	(Chakraborty et al., 2011)
Chitin nanowhiskers	59.52	(Druzian et al., 2019)
Solid waste of rosewater extraction	78.24	(Falaki and Bashiri, 2021)
AC prepared from lemon wood (ACL)	23.64	(Foroutan et al., 2021)
ACL/Fe_3O_4 magnetic nanocomposite	35.31	(Foroutan et al., 2021)
Surfactant modified activated carbon	235.7	This study

3.18. To highlight the significance of the present work, a comparative study for Langmuir adsorption capacity with previous reported adsorbents for CV dye as per table

(See Table 5.).

4. Conclusion

An investigation of CV sorption onto ACSLS found that anionic surfactant surface modification of activated carbon significantly increased the material's capacity for adsorption. The ability to adsorb substances is significantly influenced by the presence of additional salts, temperature, initial dye concentration, sorbent dose, change in pH, and period of contact. The hydrophobic characteristics of anionic surfactant are responsible for the high adsorption removal by surfactant modified AC. The hydrophobic groups in the anionic surfactant bonded to the surface of AC during surface treatment. As a result, specific binding sites based on anionic functional groups were available at the AC surface for the target removal of cationic dye (CV). Due to the surfactant's strong affinity for acid conjugate bases, good dispersion properties, and large magnitude of hydrophobic functional group rate for corresponding quantity of adsorbent, anionic surfactant modified AC was favourable in removing cationic dye. The evaluation of BET, XRD, SEM, XEDS, HR-TEM, and FTIR validated the dye sorption onto sorbent. A good concept of the optimal and stable pH for the sample solution, under which adsorption can take place, was provided by pH_{PZC} and zeta potential research. The dye removal rate of the sorbent rose with increasing pH, according to an analysis of pH variation (2–9). CV removal via ACSLS was supported at higher temperatures for the range investigated (298–318 K). Experimental data for the rate of the adsorption response showed strong agreement with pseudo 2nd order kinetics; data comparison with isotherm studies; and error analysis demonstrated good agreement with the Langmuir model. Studying thermodynamics revealed that adsorption was endothermic, with the main mechanism supporting the kinetic results being chemisorption (E_a = 45.36 KJ/mol). The column analysis that supported the Langmuir model investigation revealed the Thomas model to be suitable. Thermodynamic and temperature analyses agreed with isosteric heat analysis. Overall, it was determined that using an anionic surfactant for AC modification was a justified research decision for cationic dye adsorption.

CRediT authorship contribution statement

Rumi Goswami: Data curation. **Amit Kumar Dey:** Conceptualization, Methodology, Supervision, Data curation.

Declaration of competing Interest

The authors declare that they have no known competing financial interests or personal relationships that could have appeared to influence the work reported in this paper.

Acknowledgements

Appendix A. Supplementary material

Supplementary data to this article can be found online at https://doi.org/10.1016/j.arabjc.2022.104290.

References

Abdel-Fattah, T.M., Mohamed, T.M., Mahmoud, E., Somia, B., Matthew, A., Huff, D., James, W.L., Sandeep, K., 2015. Biochar from woody biomass for removing metal contaminants and carbon sequestration. J. Ind. Eng. Chem. 22, 103–109.

Alhogbi, B.G., Altayeb, S., Bahaidarah, E., Zawrah, M.F., 2021. Removal of anionic and cationic dyes from wastewater using activated carbon from palm tree fiber waste. Processes 9 (3), 416.

Alventosa-deLara, E., Barredo-Damas, S., Alcaina-Miranda, M.I., Iborra-Clar, M.I., 2012. Ultrafiltration technology with a ceramic membrane for reactive dye removal: Optimization of membrane performance. J. Hazard. Mater. 209–210, 492–500.

Anirudhan, T.S., Radhakrishnan, P.G., 2008. Thermodynamics and kinetics of adsorption of Cu (II) from aqueous solution onto a new cation exchanger derived from tamarind fruit shell". J. Chem. Thermodyn. 40, 702–709.

Auta, M.B.H., 2014. Hameed, Chitosan–clay composite as highly effective and low-cost adsorbent for batch and fixed-bed adsorption of methylene blue. Chem. Eng. J. 237, 350–361.

Bansiwal, A., Thakre, D., Labhshetwar, N., Meshram, S., Rayalu, S., 2009. Fluoride removal using lanthanum incorporated chitosan-beads. Colloids Sur. B 74 (1), 216–224.

Behrouz, N., Rauf, F., Bahram, A., Farzaneh, S., Bahman, R., 2018. Pb(II) and Cd (II) removal from aqueous solution, shipyard wastewater, and landfill leachate by modified Rhizopus oryzae biomass. Mater. Res. Express 5, (4) 045501.

Biswas, K., Gupta, K., Ghosh, U.C., 2009. Adsorption of fluoride by hydrous iron (III)–tin (IV) bimetal mixed oxide from the aqueous solutions. J. Chem. Eng 149 (1–3), 196–206.

Y. Bulut, H.A. Aydın. kinetics and thermodynamics study of methylene blue adsorption on wheat shells. *Desalination 194* (2006) 259–267. S.

Chakraborty, S., Chowdhury, S., Das Saha, P., 2011. Adsorption of Crystal Violet from aqueous solution onto NaOH-modified rice husk. Carbohydr. Polym. 86, 1533–1541.

Choi, H.D., Shin, M.C., Kim, D.H., Jeon, C.S., Baek, K., 2008. Removal characteristics of reactive black 5 using surfactant-modified activated carbon. Desalination 223, 290–298.

A.K. Dey, A. Dey. Selection of optimal Processing Condition during Removal of Methylene Blue Dye Using Treated Betel Nut Fibre Implementing Desirability Based RSM approach. Response surface methodology in Engineering Science (2021). ISBN: 978-1-83968-918-5.

Dey, A.K., Dey, A., 2021. Selection of optimal processing condition during removal of Reactive Red 195 by NaOH treated jute fibre using adsorption. Groundw. Sustain. Develop. 12, 100522.

Dey, A.K., Dey, A., Goswami, R., 2022. Selection of optimal performance characteristics during adsorption of Methyl red dye using sodium carbonate treated jute fibre. Desalination Water Treat. 260, 187–202.

Dey, A.K., Dey, A., Goswami, R., 2022. Adsorption characteristics of methyl red dye by Na_2CO_3-treated jute fibre using multi-criteria decision making approach. Appl. Water Sci. 12 (8), 1–22.

Dey, A.K., Goswami, R., 2022. Cationic dye removal using surface treated activated carbon as an adsorbent. Environmental Science: Water Research & Technology. https://doi.org/10.1039/D2EW00460G.

Dey, A.K., Kumar, U., 2017. Adsorption of Reactive Red 195 from polluted water upon Na$_2$CO$_3$ Modified Jute Fibre. Int. J. Eng. Technol. 9 (3S), 53–58.

Dey, A.K., Kumar, U., Dey, A., 2018. Use of response surface methodology for the optimization of process parameters for the removal of Congo Red by NaOH treated jute fibre. Desalination Water Treat. 115, 300–314.

Dey, A.K., Dey, A., Goswami, R., 2022. Fixed-bed column analysis for adsorption of Acid scarlet 3R dye from aqueous solution onto chemically modified betel nut husk fibre. Desalination Water Treat. 252, 381–390.

Dey, A.K., Kumar, U., 2017. Adsorption of anionic azo dye Congo Red from aqueous solution onto NaOH-modified jute fibre. Desalination Water Treat. 92, 301–308.

Druzian, S.P., Zanatta, N.P., Côrtes, L.N., Streit, A.F.M., Dotto, G. L., 2019. Preparation of chitin nanowhiskers and its application for crystal violet dye removal from wastewaters. Environ. Sci. Pollut. Res. 26, 28548–28557.

Elwakeel, K.Z., El-Bindary, A.A., El-Sonbati, A.Z., Hawas, A.R., 2017. Magnetic alginate beads with high basic dye removal potential and excellent regeneration ability. Can. J. Chem. 95, 807–815.

Eren, Z., Acar, F.N., 2006. Adsorption of Reactive Black 5 from an aqueous solution: equilibrium and kinetic studies. Desalination 194, 1–10.

Falaki, Z., Bashiri, H., 2021. Preparing an adsorbent from the unused solid waste of Rosewater extraction for high efficient removal of Crystal Violet. J. Iran. Chem. Soc. 18, 1–14.

Foroutan, R., Peighambardoust, S.J., Peighambardoust, S.H., Pateiro, M., Lorenzo, J.M., 2021. Adsorption of crystal violet dye using activated carbon of lemon wood and activated carbon/Fe3O4 magnetic nanocomposite from aqueous solutions: A kinetic, equilibrium and thermodynamic study. Molecules 26, 2241.

R. Foroutan, S.J. Peighambardoust, A. Ahmadi, A. Akbari, S. Farjadfard, B. Ramavandi. Adsorption mercury, cobalt and nickel with a reclaimable and magnetic composite of hydroxyapatite/ Fe$_3$O$_4$/polydopamine. 9(4) (2021) 105709

Fu, J., Chen, Z., Wang, M., Liu, S., Zhang, J., Zhang, J., Han, R., Xu, Q., 2015. Adsorption of methylene blue by a high-efficiency adsorbent (polydopamine microspheres): kinetics, isotherm, thermodynamics and mechanism analysis. Chem. Eng. J. 259, 53–61.

Ghasemi, M., Keshtkar, A.R., Dabbagh, R., Safdari, S.J., 2011. Biosorption of uranium (VI) from aqueous solutions by Ca-pretreated Cystoseira indica alga: breakthrough curves studies and modeling. J. Hazard. Mater. 189, 141–149.

Gobi, K., Mashitah, M.D., Vadivelu, V.M., 2011. Adsorptive removal of methylene blue using novel adsorbent from palm oil mill effluent waste activated sludge: equilibrium, thermodynamics and kinetic studies. Chem. Eng. J. 171, 1246–1252.

Gohr, M.S., Abd-Elhamid, A.I., El-Shanshory, A.A., Soliman, H.M., 2022. Adsorption of cationic dyes onto chemically modified activated carbon: Kinetics and thermodynamic study. J. Mol. Liq. 346, 118227.

Goswami, R., Dey, A.K., 2022. "Positive Impact of Environment due to Covid-19 lockdowns in parts of India: a review". Environ. Eng. Manage. J. 21 (4), 559–568.

Goswami, R., Dey, A.K., 2022. Use of anionic surfactant-modified activated carbon for efficient adsorptive removal of crystal violet dye. Adsorp. Sci. Technol., 2357242

Hailu, S.L., Nair, B.U., Mesfin, R.A., Diaz, I., Tessema, M., 2017. Preparation and characterization of cationic surfactant modified zeolite adsorbent material for adsorption of organic and inorganic industrial pollutants. J. Environ. Chem. Eng. 5, 3319–3329.

Ho, Y.S., Chiang, T.H., Hsueh, Y.M., 2005. Removal of basic dye from aqueous solution using tree fern as a biosorbent. Process. Biochem. 40 (1), 119–124.

Ho, Y.S., McKay, G., 1999. Pseudo-second-order model for sorption processes. Process. Biochem. 34 (5), 451–465.

Hoang, B.N., Nguyen, T.T., Bui, Q.P.T., Bach, L.G., Vo, D.V.N., Trinh, C.D., Bui, X.T., Nguyen, T.D., 2020. Enhanced selective adsorption of cation organic dyes on polyvinyl alcohol/agar/maltodextrin water-resistance biomembrane. J. Appl. Polym. Sci. 137, 48904.

Homagai, P.L., Poudel, R., Poudel, S., Bhattarai, A., 2022. Adsorption and removal of crystal violet dye from aqueous solution by modified rice husk. Heliyon 8 (4), e09261.

Jiménez-Castañeda, M., Medina, D., 2017. Use of surfactant-modified zeolites and clays for the removal of heavy metals from water. Water 9, 235.

Kannan, N., Sundaram, M.M., 2001. Kinetics and mechanism of removal of methylene blue by adsorption on various carbons—a comparative study. Dye Pigment 51, 25–40.

Kapoor, A., Yang, R.T., 1989. Correlation of equilibrium adsorption data of condensable vapours on porous adsorbents. Gas Sep. Purif. 187–192.

Karaca, S., Gürses, A., Açıkyıldız, M., Ejder, M.K., 2008. Adsorption of cationic dye from aqueous solutions by activated carbon. Micropor. Mesopor. Mater. 115, 376–382.

Lagergren, S., 1898. About the theory of so called adsorption of solute substances. Ksver Veterskapsakad Handl 24 (4), 1–39.

Lataye, D.H., Mishra, I.M., Mall, I.D., 2009. Adsorption of α-picoline on granular activated carbon and rice husk ash from aqueoussolution: equilibrium and thermodynamic study. Chem. Eng. J. 147 (2–3), 139–149.

Lataye, D.H., Mishra, I.M., Mall, I.D., 2011. Removal of 4-picoline from aqueous solution by adsorption onto bagasse fly ash and rice husk ash: equilibrium, thermodynamic and desorption study. J. Environ. Eng. 137 (11), 1048–1057.

S.Y. Lin, W.F. Chen, M.T. Cheng, Q. Li. Investigation of factors that affect cationic surfactant loading on activated carbon and perchlorate adsorption. Colloids Surf. A Physicochem. Eng. Asp. 434(2013) 236–242. [CrossRef].

Loulidi, I., Boukhlifi, F., Ouchabi, M., 2020. Adsorption of CV onto an agricultural waste residue: kinetics, isotherms, thermodynamics and mechanism of adsorption. Scient. World J., 5873521

Madhavakrishnan, S., Vasanthakumar, R., Manickavasagam, K., 2009. Adsorption of crystal violet dye from aqueous solution using Ricinues communis pericarp carbon as an adsorben. E-J. Chem. 6 (4), 1109–1116.

Marquardt, D.W., 1963. An algorithm for least squares estimation of nonlinear parameters. J. Soc. Ind. Appl. Math. 11 (2), 431–441.

Mouni, L., Belkhiri, L., Bollinger, J.C., Bouzaza, A., Assadi, A., Tirri, A., Dahmoune, F., Madani, K., Remine, H., 2018. Removal of Methylene Blue from aqueous solution by adsorption on Kaolin: kinetic and equilibrium studies. Appl. Clay Sci. 153, 38–45.

Muthukumaran, C., Sivakumar, V.M., Thirumarimurugan, M., 2016. Adsorption isotherms and kinetic studies of crystal violet dye from aqueous solution using surfactant modified magnetic nanosorbent. J. Taiwan Inst. Chem. Eng. 63, 354–362.

C. Namasivayam, M.V. Suresh Kumar. Removal of chromium (VI) from water and wastewater using surfactant modified coconut coir pith as a biosorbent. Bioresour. Technol. 99(2008)2218–2225.

A. S. Omer, G. A. El. Naeem, A. L. Abd-Elhamid, A. A. Nayl, Adsorption of crystal violet and methylene blue dyes using a cellulose-based adsorbent from sugarcane bagasse: characterization, kinetic and isotherm studies. Journal of Materials Research and Technology. 2022, 19, 3241-3254.

Onal, Y., 2006. Kinetics of adsorption of dyes from aqueous solution using activated carbon prepared from waste apricot. J. Hazard. Mater. B137 (3), 1719–1728.

S.J. Peighambardoust, R. Foroutan, S.H. Peighambardoust, H. Khatooni, B. Ramavandi. Decoration of Citrus limon wood carbon with Fe$_3$O$_4$ to enhanced Cd^{2+} removal: A reclaimable and magnetic nanocomposite. 282 (2021) 131088

G.S.D. Reis, S.H. Larsson, M. Thyrel, T.N. Pham, E.C. Lima, H.P.D. Oliveira, G. L. Dotto. Preparation and application of Efficient

Biobased Carbon Adsorbents Prepared from Spruce Bark Residues for Efficient Removal of Reactive Dyes and Colors from Synthetic Effluents. Coatings. 772 (2021) 11(7).

Satapathy, M.K., Das, P., 2014. Optimization of crystal violet dye removal using novel soil-silver nanocomposite as nanoadsorbent using response surface methodology. J. Environ. Chem. Eng. 2, 708–714.

Sun, D., Zhang, X., Wu, Y., Liu, X., 2010. Adsorption of anionic dyes from aqueous solution on fly ash. J. Hazard. Mater. 181, 335–342.

Tan, I.A.W., Ahmad, A.L., Hameed, B.H., 2008. Adsorption of basic dye on high-surface area activated carbon prepared from coconut husk: equilibrium, kinetic and thermodynamic studies. J. Hazard. Mater. 154, 337–346.

Verma, A.K., Dash, R.R., Bhunia, P., 2012. A review on chemical coagulation/flocculation technologies for removal of colour from textile wastewaters. J. Environ. Manag. 93, 154–168.

Wang, W., Huang, G., An, C., Zhao, S., Chen, X., Zhang, P., 2018. Adsorption of anionic azo dyes from aqueous solution on cationic gemini surfactant-modified flax shives: synchrotron infrared, optimization and modeling studies. J. Clean. Prod. 172, 1986–1997.

Wong, Y.C., Szeto, Y.S., Cheung, W.H., McKay, G., 2004. Adsorption of acid dyes on chitosan—equilibrium isotherm analyses. Process. Biochem. 39, 695–704.

Wu, S.H., Pendleton, P., 2001. Adsorption of anionic surfactant by activated carbon: effect of surface chemistry, ionic strength, and hydrophobicity. J. Colloid Interface Sci. 243, 306–315.

Yagub, M.T., Sen, T.K., Ang, H.M., 2012. Equilibrium, kinetics, and thermodynamics of methylene blue adsorption by pine tree leaves. Water Air Soil Pollut. 223, 5267–5282.

Yagub, M.T., Sen, T.K., Afroze, S., Ang, H.M., 2014. Dye and its removal from aqueous solution by adsorption: a review. Adv. Colloid Interface Sci. 209, 172–184.

Yu, S., Liu, M., Ma, M., Qi, M., Lü, Z., Gao, C., 2010. Impacts of membrane properties on reactive dye removal from dye/salt mixtures by asymmetric cellulose acetate and composite polyamide nanofiltration membranes. J. Membr. Sci. 350, 83–91.

Zhou, Y., Wang, Z., Andrew, H., Ren, B., 2018. Gemini surfactant-modified activated carbon for remediation of hexavalent chromium from water. Water 10, 91.